NASA CR 54183

FINAL REPORT

RCA SUPERCONDUCTIVE PRODUCTS

HIGH MAGNETIC FIELD SUPERCONDUCTING PROPERTIES OF Nb_3Sn FILMS

by

N. S. Freedman (Project Supervisor), H. C. Schindler
(Project Engineer) F. R. Nyman, and K. Strater

prepared for

NATIONAL AERONAUTICS AND SPACE ADMINISTRATION

August 1965

CONTRACT NAS 3-4113

TECHNICAL MANAGEMENT
NASA LEWIS RESEARCH CENTER
CLEVELAND, OHIO
SPACECRAFT TECHNOLOGY DIVISION

PROJECT MANAGER — A. E. ANGLIN
TECHNICAL ADVISOR — J. C. LAURENCE

RADIO CORPORATION OF AMERICA
ELECTRONIC COMPONENTS AND DEVICES, HARRISON, N.J.

NOTICE

This report was prepared as an account of Government-sponsored work. Neither the United States, nor the National Aeronautics and Space Administration (NASA), nor any person acting on behalf of NASA:

a) Makes any warranty or representation, expressed or implied, with respect to the accuracy, completeness, or usefulness of the information contained in this report, or that the use of any information, apparatus, method, or process disclosed in this report may not infringe privately-owned rights; or

b) Assumes any liabilities with respect to the use of, or for damages resulting from the use of any information, apparatus, method or process disclosed in this report.

As used above, "person acting on behalf of NASA" includes any employee or contractor of NASA, or employee of such contractor, to the extent that such employee or contractor of NASA, or employee of such contractor prepares, disseminates, or provides access to, any information pursuant to his employment or contract with NASA, or his employment with such contractor.

Requests for copies of this report should be referred to:

National Aeronautics and Space Administration
Office of Scientific and Technical Information
Washington, D. C. 20546

Attention: AFSS-A

NASA CR 54183

FINAL REPORT

HIGH MAGNETIC FIELD SUPERCONDUCTING PROPERTIES OF Nb_3Sn FILMS

by

N. S. Freedman (Project Supervisor), H. C. Schindler
(Project Engineer) F. R. Nyman, and K. Strater

prepared for

NATIONAL AERONAUTICS AND SPACE ADMINISTRATION

August 1965

CONTRACT NAS 3-4113

TECHNICAL MANAGEMENT
NASA LEWIS RESEARCH CENTER
CLEVELAND, OHIO
SPACECRAFT TECHNOLOGY DIVISION

PROJECT MANAGER — A. E. ANGLIN
TECHNICAL ADVISOR — J. C. LAURENCE

HIGH MAGNETIC FIELD SUPERCONDUCTING PROPERTIES OF Nb_3Sn FILMS

by

N. S. Freedman (Project Supervisor), H. C. Schindler (Project Engineer), F. R. Nyman, and K. Strater

ABSTRACT

10448

The shielding characteristics of niobium-stannide layers varying in thickness and critical current, deposited on the exterior of steatite, Hastelloy, and nickel cylinders were investigated. Maximum magnetic fields shielded in this fashion free from flux jumps were two kilogauss. Stacked discs of concentric rings of niobium-stannide shielded 12 kilogauss free from flux jumps in a 0.500-inch inside diameter. This principle of concentric niobium-stannide rings is equally well adaptable to other superconductive devices where flux jumps have been a major problem. Electron bombardment of niobium-stannide with an integrated flux density of 10^{18} electron/cm^2 produced a 50 percent reduction in critical current. No deleterious effects on the niobium-stannide were observed below the cumulative 10^{18} electron/cm^2 density level.

author

TABLE OF CONTENTS

TABLE OF CONTENTS (Continued)

TABLE OF CONTENTS (Continued)

LIST OF ILLUSTRATIONS

LIST OF ILLUSTRATIONS (Continued)

LIST OF TABLES

HIGH MAGNETIC FIELD SUPERCONDUCTING PROPERTIES OF Nb_3Sn FILMS

by

N. S. Freedman (Project Supervisor), H. C. Schindler (Project Engineer), F. R. Nyman, and K. Strater

I. SUMMARY

Under this contract NAS 3-4113 for NASA, Lewis Research Center, RCA has been engaged in an evaluation of the electromagnetic properties of niobium-stannide films for high magnetic field devices. Progress under this contract has established the following:

1. That the low-field electromagnetic instability encountered in the construction of superconductive magnets is equally troublesome in the construction of other superconductive film devices.

2. That the instabilities in the low-field region can be minimized by (a) plating the Nb_3Sn layer with silver, (b) decreasing the thickness of the Nb_3Sn layer, and (c) optimizing the width of the Nb_3Sn coating.

3. That bombardment of niobimm-stannide with a cumulative electron density below 10^{17} electron/cm^2 does not deteriorate its electromagnetic performance. However, when the integrated electron density is increased to the 10^{18} electron/cm^2 level, the critical current of the niobium-stannide is degraded 50 percent.

Under this contract, the following specific accomplishments were achieved:

1. Single-phase β-tungston structure niobium-stannide was vapor-deposited on a variety of substrates such as steatite, Hastelloy, nickel and platinum. Shielding characteristics varied depending upon the substrate.

2. Equipment was developed for vapor depositing single-phase niobium-stannide on 1-inch and 2-inch flats and 1/4 to 1/2-inch O.D. cylinders.

3. Stable shielding, (i.e., free from flux jumps) of low

magnetic fields (0 to 2 kilogauss) was realized only with thin deposits (.0005 to .002-inches thick niobium-stannide layers).

4. Stability of the niobium-stannide layer correlated with the thickness of the deposit, critical current, rate of field application, substrate, and quality of silver plating.

5. Equipment was developed for vapor-depositing single-phase niobium-stannide continuously on a 2-inch wide ribbon.

6. A 12-kilogauss field was shielded free from flux jumps in a series of stacked discs of concentric niobium-stannide rings, 0.500-inch inside diameter, 1.875-inch outside diameter, and 0.791 inches long.

II. INTRODUCTION

A. BACKGROUND

Early in 1961, while working under a basic research program on superconductivity sponsored in part by the Air Force System Command[1], RCA Laboratories developed a high temperature gas-phase reaction process for depositing single-phase, superconductive niobium-stannide (Nb_3Sn) continuously on platinum wire or ribbon[2].

The film deposition process consists of continuously feeding premixed $SnCl_2$ and $NbCl_5$ at a controlled rate into a vaporization chamber maintained above 500°C. Hydrogen and helium are added downstream to the gaseous metal chlorides and the gaseous mixture is then fed into the deposition chamber. The sample being coated with Nb_3Sn is maintained at temperatures ranging from 700°C to 900°C depending on the deposition rate desired.

RCA Laboratories had further explored this process and prior to this contract developed techniques for depositing homogeneous deposits of Nb_3Sn on flat and cylindrical geometries on varieties of metal and insulator substrates[3]. Nb_3Sn films ranging in thickness from 0.2 to 30 mils (0.0002 to 0.030 inch) were deposited on flat Hastelloy and ceramic substrates. The Nb_3Sn deposits exhibited critical temperatures ranging from 17.6 to 18.3°K and transition widths from 0.04 to 0.4°K. Adherence of the Nb_3Sn films to the various substrates was excellent. Superconducting current densities of 3×10^5 amps/cm^2 in a 90-kilogauss background field were attained.

In addition to depositing adherent superconductive Nb_3Sn films on metal and insulator substrates, Nb_3Sn was also deposited on the inside surface of quartz tubes up to 25mm in diameter. On cooling, the Nb_3Sn separated from the quartz leaving a pure unsupported Nb_3Sn tube. Nb_3Sn tubes up to 50 mils thick were made in this manner.

These deposited Nb_3Sn films are also amenable to fabrication techniques for precisely forming or "printing" intricate patterns of superconductive Nb_3Sn.

Nb_3Sn was deposited on 1-inch wide platinum substrate, and using photo-etching techniques, concentric Nb_3Sn ring patterns were etched out on each side of the tape. When a series of these discs were stacked and placed in a magnetic field, supercurrents were induced in the rings, and high fields were shielded that were rela-

tively free from flux jumps. Prior to this contract maximum field shielded in this manner in a multiple stack arrangement 2.1-cm long, 2.5-cm O.D., and 0.5-cm I.D. was 60 kilogauss[4].

In studying the effects of neutron radiation on Nb_3Sn, RCA had found that[5,6]:

1. the current density of Nb_3Sn increases;
2. the stability of the Nb_3Sn layer decreases.

These effects were attributed to the additional dislocations induced into the Nb_3Sn structure.

It is expected that work covered under this contract will make possible the utilization of superconductive Nb_3Sn layers with intricate geometries which will find applications in shielding, flux pumping, field shaping and energy storage devices.

B. CONTRACT NAS 3-4113

A major objective of this contract was to investigate the electromagnetic properties of niobium-stannide films for potential high magnetic field devices. An additional aim was to investigate the effects of electron bombardment on the Nb_3Sn films. (Work was already underway at RCA on neutron radiation effects.) These objectives have been attained and are described in the following pages. Section III details the process for depositing Nb_3Sn on cylinders and the electromagnetic evaluation of Nb_3Sn layers. Section IV deals with the continuous and uniform deposition of Nb_3Sn on 2-inch wide ribbon. Also described is the stacked concentric Nb_3Sn ring disc approach for either alleviating or minimizing the flux jumping problem. In Section V the effects of electron bombardment on the superconductive properties of Nb_3Sn are described, and Section VI discusses some applications of the stacked discs of concentric Nb_3Sn rings for high field superconductive devices.

III. DEPOSITION PROCESS AND ELECTROMAGNETIC EVALUATION OF Nb_3Sn LAYERS

A. PROCESS

The original vapor-deposition apparatus for growing niobium-stannide on cylinders and flats is shown in Figure 1.

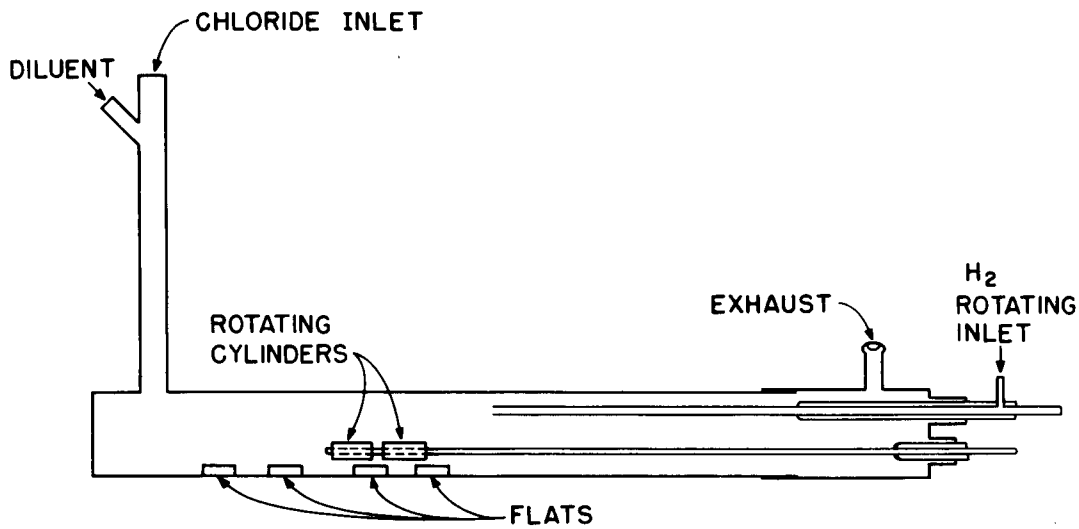

FIG. I STATIC FILM DEPOSITION APPARATUS

The substrate is first ground to the desired size and then ultrasonically cleaned. The substrate is immersed and maintained at the same temperature as the deposition chamber. The furnace temperatures are controlled to within plus or minus ten degrees centigrade. The entire deposition apparatus is flushed for approximately one hour with helium prior to beginning the niobium-stannide deposition.

Niobium pentachloride and tin dichloride in a 50 percent molecular ratio are injected by a screw mechanism into the deposition chamber. The metal chlorides are volatilized at temperatures ranging from 800 to 900°C at the inlet end of the reaction tube and transported toward the substrate samples by the helium diluent gas (Figure 1). Hydrogen is introduced through a rotating tube which swirls the gas to assure thorough mixing of the reacting gases in the area of the substrate to be coated with Nb_3Sn. The chlorides and hydrogen react at the hot surface of the substrates to form a homogeneous adherent Nb_3Sn film. The unused gases and reaction by-products are exhausted at the opposite end of the inlet. The deposition temperature ranges from 800 to 900°C. The overall

chemical reaction is as follows:

$$3Nb\ Cl_5 + Sn\ Cl_2 + 8\tfrac{1}{2}\ H_2 \xrightarrow{\Delta} Nb_3Sn + 17\ HCl$$

During a typical deposition run the gaseous atmospheres were as follows:

Gas	Molecular Concentration
Helium	0.75 moles/hour
Hydrogen	2 moles/hour
Niobium Pentachloride	0.055 moles/hour
Tin Dichloride	0.055 moles/hour

The original vapor-deposition apparatus was modified after run No. 21 to accommodate larger diameter cylinders and flats. The uniformity of the Nb_3Sn deposit was also improved by (1) incorporating a mixing chamber where the powder metal chlorides are volatilized and (2) allowing sufficient residence time in the mixing chamber to dampen the fluctuations in powder-feed rate, and (3) replacing the rotating hydrogen inlet by injecting the hydrogen in the immediate vicinity of the substrate sample. The modified static film deposition apparatus is shown in Figure 2.

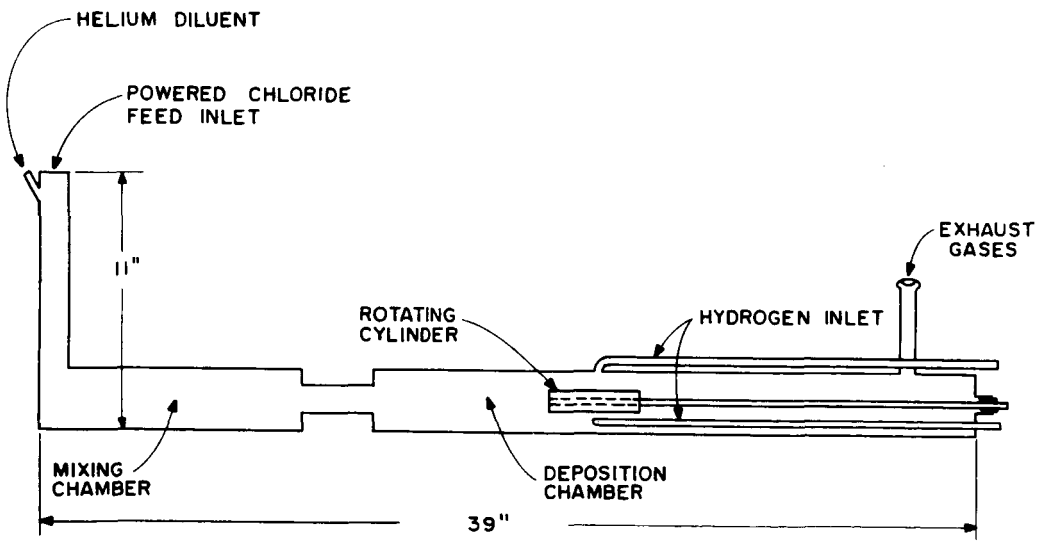

FIG. 2 Nb_3Sn VAPOR DEPOSITION CHAMBER

A summary of all deposition conditions and an electromagnetic evaluation of the Nb_3Sn layers is presented in Table 1. With this apparatus, niobium-stannide was deposited on flats up to 1-inch wide by 2 inches long and on cylinders up to ½-inch diameter. Good adherent Nb_3Sn deposits were obtained on steatite, Hastelloy, nickel and platinum substrates.

TABLE I

SUMMARY OF DEPOSITION CONDITIONS AND ELECTROMAGNETIC EVALUATION OF Nb_3Sn LAYERS

Run No.	Dep. Temp. °C	Feed Rate Gm/Hr	Dep. Time, Hrs	Sample No.	Substrate Material	Substrate O. D. Inch	Dep_3 10 Inch	Field Shielded kG	Extrapo. Shielded Field kG	α kG-amp. cm^2	B_8 kG	Type of Shielding	Rate of Field Appl. Gauss/Sec	Plating	Plating Rate Amp/Ft^2
28055 #1	800	-	2-1/2		Hastelloy	0.250	0.3			No Significant Shielding				None	
				4	Steatite Flats	0.250	1.0	.7				Unstable	16	None	
28055 #2	800	-	1-1/2		Hastelloy	0.250	0.3	-				Unstable	16	None	
				2	Steatite Flats	0.250	0.3			No Significant Shielding					
28055 #3	800	4.09	2-3/4		Hastelloy	0.250	0.3			No Significant Shielding					
				3	Steatite Flats	0.250	0.1			No Significant Shielding					
28055 #4	800	3.5	6		Hastelloy	0.250	0.1			No Significant Shielding					
					Steatite Flats	0.250	0.3			No Significant Shielding					
28055 #5	900	3.59	6-1/2		Hastelloy	0.250	1.0			No Significant Shielding					
				1	Steatite Flats	0.250	0.5			No Significant Shielding					
28055 #6	900	3.59	3	5	Hastelloy	0.250	1.0			No Significant Shielding					
				7	Steatite Flats	0.250	0.5			No Significant Shielding					
28055 #7	900	4.39	6	6	Hastelloy	0.250	0.6			No Significant Shielding					
					Steatite Flats	0.250									
28055 #8	900	10.5	7-1/2	8	Hastelloy	0.250	1.3	1.0		1.07	3.4	Stable	50	None	
				9	Steatite Flats	0.250	1.0	1.4		4.7	10.0	Unstable	13	Ag.	33
28055 #9	Unsatis.Run														
28055 #10	900	10.5	7-1/2	10	Hastelloy	0.250	2.0	1.5		0.53	1.7	Stable	500	None	
				11	Steatite Flats	0.250	1.1	1.3		2.4	2.2	Partially Stable	16	None	
28055 #11	900	14.5	3-3/4	12	Hastelloy	0.250	1.7	1.1		.90	3.3	Stable	350	None	
				13	Steatite Flats	0.250	0.6	Unstable		-	-	Unstable	50	None	
28055 #12	900	10.0	2-1/2		Hastelloy	0.250		Dep.Flaked off							
				14	Steatite Flats	0.250	0.5	1.0		5.3	6.7	Unstable	8	None	
28055 #13	900	17	7-3/4		Hastelloy	0.250		Dep.Flaked off							
				15	Steatite Flats	0.250	2.5	1.7		Unstable	Unstable	Unstable	5	None	
28055 #14	900	14.5	3.3	14	Steatite[1]	0.250	2.1	Unstable	→				8.0	None	-
				14	Steatite[1]	0.250	2.1	Unstable	→				8.0	Ag	33
				18	Steatite Flats[2]	0.250	1.3	-		4.6	8.5	Unstable	8.0	None	-
28055 #15	900	24.0	2.0	16	Steatite	0.250	0.7	1.3	1.8	5.3	5.4	Part.Stable	10.0	None	-
				17	Steatite[3]	0.250	0.75	2.4	2.5	4.8	0.46	Unstable	7.0	None	-
				17	Steatite[4]	0.250	0.75	1.7	1.64	4.5	6.6	Unstable	9.0	None	-
28055 #16	900	28.0	2.5		Hastelloy	0.250	Deposit Flaked Off →								
						0.25	No Significant Shielding →						8.0	None	-
28055 #17	900	30.0	0.5	19	Hastelloy	0.250	0.25	No Significant Shielding →					8.0	None	-
				20	Nickel	0.250	1.5	Unstable →					7.0	None	-
				20	Nickel	0.250	1.5	1.6	1.9	2.16	5.5	Stable	5.0	Ag	53
28055 #18	900	12.7	3.0		Hastelloy	0.250	Deposit Flaked Off →								
					Hastelloy	0.250	Deposit Flaked Off →								
28055 #19	900	12.7	1.5	21	Hastelloy	0.250	1.0	1.6		1.2	1.0	Stable	8.0	None	-
				21	Hastelloy	0.250	1.0	1.6		1.2	1.0	1 Jump	250.0	None	-
28055 #20	Unsatisfactory Deposition-Air Leak in System														
28055 #21	900	15.2	1.0	22	Hastelloy	0.375	0.5	Unstable →					7.0	None	-
				22	Hastelloy	0.375	0.5	2.2	2.8	16.6	9.7	Part.Stable	8.0	Ag	33
				23	Hastelloy	0.375	0.75	2.2	2.2	3.4	3.8	Part.Stable	8.0	None	-
				23	Hastelloy	0.375	0.75	1.8	-	2.9	3.6	Stable	8.0	Ag	-
28055 #22	900	50.0	1.25	24	Hastelloy	0.375	2.4	Unstable →					8.0	None	-
				24			2.4	Unstable →					8.0	Ag	33
				24A			0.25	Not Measured →							
28055 #23	Unsatisfactory Deposition														
28055 #24	900	19.0	2.0	25	Hastelloy	0.500	1.1	1.2	1.82	1.0	1.0	Part.Stable	8.0	None	-
				25	Hastelloy	0.500	1.0	1.2	1.82	1.2	1.0	Almost Stable	8.0	Ag	33
				25	Hastelloy	0.500	1.1	1.5	1.89	1.4	1.0	Stable	8.0	Ag	5
				25	Hastelloy	0.500	1.1	1.5	1.89	1.4	1.0	Stable	34.0	Ag	5
				26	Nickel	0.500	2.3	Unstable →					8.0	None	-
				26	Nickel	0.500	2.3	5.0	8.0	8.3	7.5	Unstable	8.0	Ag	33
							2.3	3.0	6.7	12.0	16.5	Part.Stable	8.0	Ag	5
28055 #25	Run Conducted To Obtain Short-Sample Specimens														
28055 #26	900	25.0	2.0	27	Platinum	0.250	2.0	3.6	5.7	5.7	6.1	Part.Stable	5.0	None	-
							2.0		5.7	5.7	6.1	Stable	500.0	Ag	33
28055 #27	900	18.0	2.0	28	Platinum	0.250	1.6	3.0	5.0	3.8	3.95	Part.Stable	5.0	None	-
				29	Platinum	0.250	0.8	1.2	1.2	1.8	3.65	Stable	5.0	None	-
28055 #29	900	18.0	1.0	30	Platinum	0.250	0.6	2.2	2.9	17.3	10.0	Part.Stable	5.0	None	-
								2.0	2.6	16.8	10.0	Stable	5.0	Ag	33
				31	Platinum	0.250	0.6	2.0	2.1	8.9	7.5	Stable	5.0	None	-
				31	Platinum	0.250	0.6	2.0	2.1	8.9	7.5	Stable	5.0	Ag	33

[1]Steatite cylinders from run #12 plated with nickel strike and additional Nb_3Sn deposited. [2]Flats from run 28055 #8 platinum plated and additional Nb_3Sn deposited. [3]Circular rings were cut into steatite cylinder. [4]All Nb_3Sn not in groves was removed.

X-ray diffraction patterns of the lattice show the niobium-stannide on the steatite, platinum, nickel and Hastelloy to be single-phase with lattice constants ranging between 5.289 to 5.290^{o}A. The experimental technique for determining the X-ray patterns consisted of scraping niobium-stannide from the substrate and obtaining powder film patterns using 2 radian cameras with Cu/Ni radiation. The lattice constants were obtained using a RCA 601 computer in conjunction with a program incorporating Cohen's method of least squares[7]. Only the back reflection lines having double angles greater than 120^{o} were used in calculating the lattice parameters. The diffraction lines on the films were measured with vernier and millimeter scales.

B. THEORETICAL CONSIDERATIONS

1. Introduction

When a superconducting ring or cylinder is placed in a background field, H, supercurrents are induced in the ring or cylinder and the superconductor shields the magnetic field from the interior until the critical current of the superconductor is reached. At this field, penetration takes place (neglecting flux jumps) and the amount of shielding decreases monotonically as the applied field is increased further (at higher fields the critical current is lower). If the superconductive layer on the cylinder reverts momentarily to the normal state, the entire external magnetic field penetrates the cylinder and no shielding is exhibited by the cylinder. As the field is further increased, the cylinder starts shielding the background field again. Momentary reversion to the normal state is referred to as a flux jump[8]. Factors effecting initiation of the flux jumps will be discussed later. The shielding characteristics of a cylinder tested under conditions where no flux jumps occurred is shown in Figure 3. The dotted line is the shielding behavior of the same cylinder when tested in an environment favorable to flux instabilities.

2. Shielding Behavior of Long Hollow Nb_3Sn Cylinders

Kim and coworkers[8] found that the local magnetization (difference in gauss between the internal and external fields) measured at the center of the tube could be derived from an induced supercurrent density with a critical value given by:

$$J_C = \frac{\alpha}{B_o + H} \qquad (1)$$

where α and B_o are constant and H is perpendicular to J. In the region of low current density J, and high fields H, the term

$$\alpha = JH = \text{constant} \quad (H >> B_o) \qquad (2)$$

takes on the physical significance of the Lorentz force which determines the superconductive to normal transition state.

If a uniform magnetic field H is applied parallel to the axis of a long hollow Nb_3Sn cylinder of outer radius a, inside radius b, and wall thickness w, the flux density at any radial point r is determined completely through the relations:

$$B = H + 4\pi m$$

$$J(B) = c\nabla \times m \qquad (3)$$

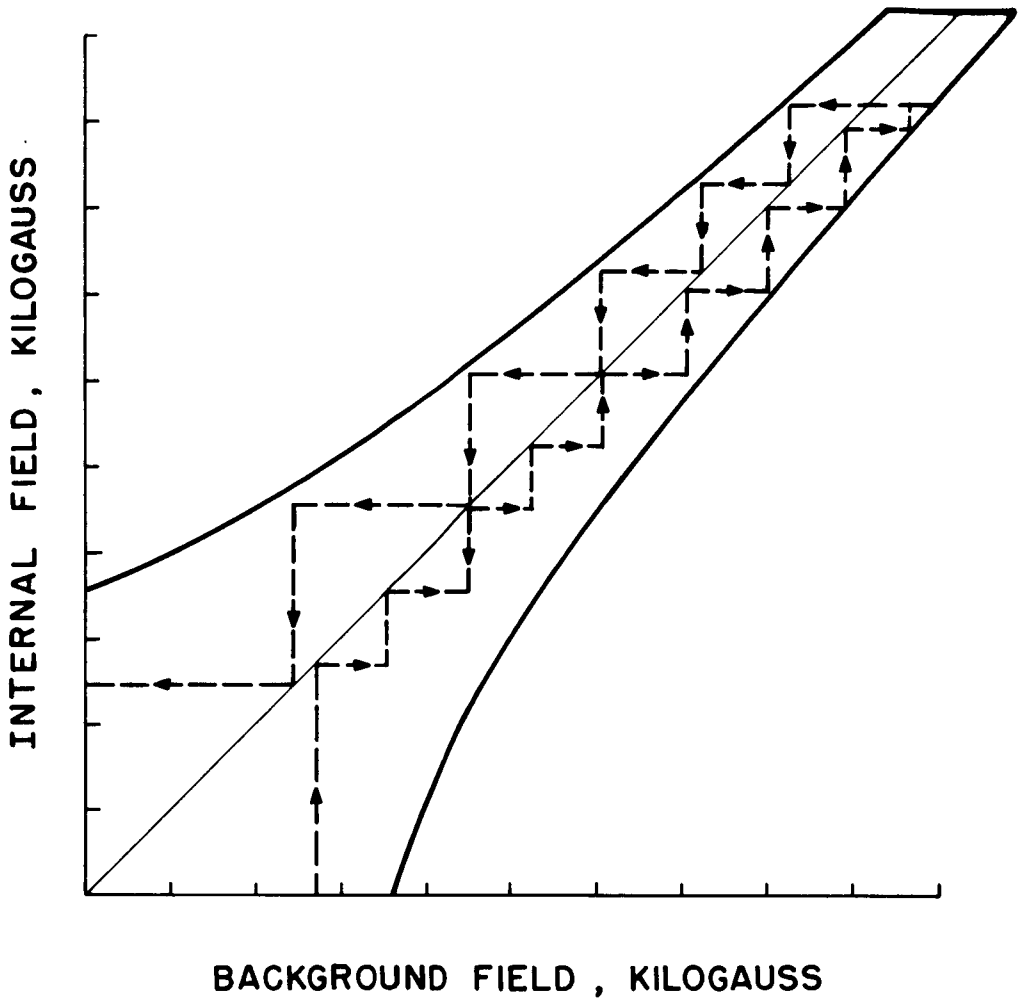

FIG. 3 CRITICAL STATE CURVE

which reduces to the scalar equation:

$$B(r) = H + m(r) \qquad (4)$$

where m (r) is the magnetization.

The field value of the center (r = 0) is the measurable quantity, H. When the sample is in the critical state, for a given field-dependent critical current density J_c (B) equation (4) becomes:

$$H' = H + k \int_b^a J_c \left[B(r) \right] dr = H + k\, w\, j \qquad (5)$$

where k = 0.4 gauss-cm/A and J is an average current density. Elimination of r leads to the integral relations:

$$k = \int_{H^* - \frac{1}{2}M}^{H^* + \frac{1}{2}M} \frac{dB}{J\ (B)} = \int_{H}^{H'} \frac{dB}{J\ (B)} \qquad (6)$$

where $H^* = \frac{1}{2}\ (H' + H)$ is the mean field in the sample wall, and $M = H' - H$ is the field produced by the induced supercurrent. Equation (5) relates the critical current density J(B) to observable experimental variable: H, H' and w. Using (1) in (6) one obtains:

$$k = \int_{H}^{H'} \frac{(B_o + H)\ dB}{\alpha} \qquad (7)$$

integrating:

$$\alpha k w = (H' - H)\ B_o + \tfrac{1}{2}\ (H'^2 - H^2) \qquad (8)$$

or:

$$\alpha k w = (H' - H) \left[B_o + \frac{H' + H}{2} \right] \qquad (9)$$

Recalling the definition of M and H*, (8) becomes

$$\alpha k w = M\ (B_o + H^*) \qquad (10)$$

indicating that if (1) is valid, 1/M should be linear in H*. Thus, an experimental plot of 1/M vs. H* allows us to verify the form of (1) in addition to evaluating the constants α and B_o.

C. ELECTROMAGNETIC EVALUATION

1. Testing Procedure

a. Cylinder Evaluation

The shielding characteristics of the Nb_3Sn layer on cylinders were measured in a 30-kilogauss, all niobium-stannide ribbon magnet. This superconductive magnet was 5½ inches long, had a 1¼-inch diameter and provided a 3-inch axial field uniformity of ±2½ percent. The magnetic field inside and outside the cylinder under test is measured with a SBV522 Hall probe and recorded on an X-Y recorder. The physical arrangement of the Hall probe, test cylinder, and magnet is shown in Figure 4.

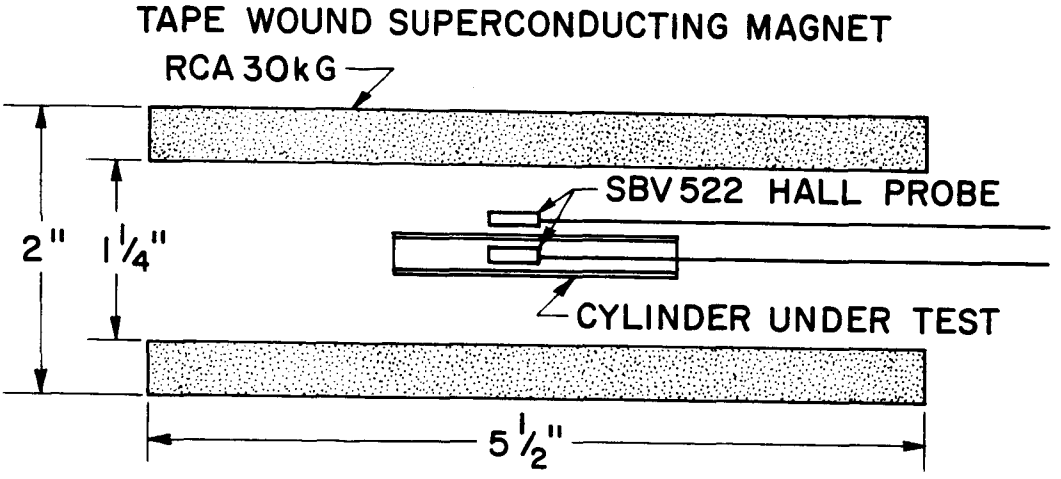

FIG.4 SCHEMATIC OF CYLINDER TESTING APPARATUS

The current into the magnet is controlled by a rate control assembly consisting of a variable direct current motor driving a 25-turn helipot. This permits the variation of the magnetic field from 0-30 kilogauss at rates varying from 3 gauss/sec. to 500 gauss/sec.

b. Short Sample Tests

The critical current-magnetic field characteristics of the sample under test is measured in a background field up to 30 kilogauss using test samples as shown in Figure 5.

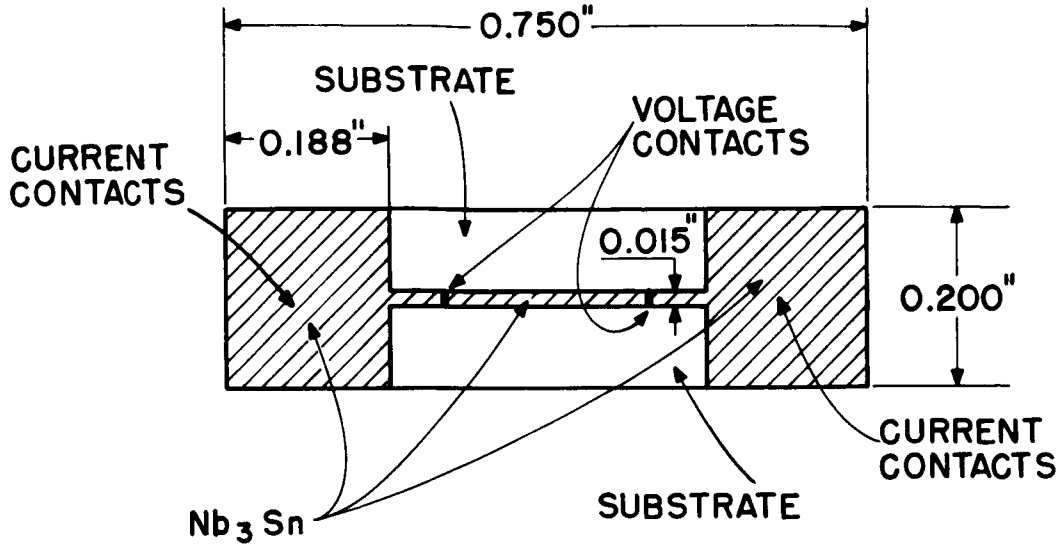

FIG.5 TEST SAMPLE

The large areas are used for current contacts and voltage probes are placed at the extremities of the 15-mil wide strip. Normalcy is considered to occur when the voltage across the superconductor just exceeds 10 microvolts. The current and magnetic field are both rate controlled and critical points are determined by both maintaining a constant critical field while increasing the current, and by maintaining a constant critical field while increasing the magnetic field. To determine current densities, accurate cross sections are obtained from metallographic cross section measurements.

2. Shielding Characteristics of Cylinder and Factors Influencing Flux Jumps

a. Concept of Stable Shielding

Niobium-stannide can be vapor-deposited with relative ease in thicknesses ranging from a minimum of a fraction of a mil (<.001 inch) to a maximum of 50 to 100 mils on flats and exterior of cylinders. Heavy deposits of niobium-stannide are grown with relative ease on both metallic and insulator substrates. To date, however, all heavy deposits have exhibited large flux jumps, predominately in the low-magnetic-field regions. In order to overcome the low-field instabilities, efforts were focused initially on depositing a multilayer structure on Hastelloy and steatite cylinders consisting of several thin, stable layers. Each individual layer was either inherently stable or stabilized by metal plating on the surface. To establish the thickness per layer, thin deposits ranging from 0.5 to 2.5 mils in thickness were grown. In the first few experimental runs, attempts were made to grow extremely thin deposits on both Hastelloy and steatite substrates (Run 28055, No. 1 through 7). In thin deposit thicknesses of only 0.1 to 0.4 mils, no significant shielding was observed. In later experimental runs, deposit thicknesses were increased up to 2.5 mils. The heavier deposits shielded a maximum of 1.7 kilogauss; however, flux jumps were present in the low-field region. With steatite cylinders, flux jumps and field instabilities were present when the deposits were as thin as 0.5 mils and the value of α, a material constant was only 5.3×10^6 kG-amp/cm^2. In these tests the field was only increased at 15 gauss/second. In contrast, a Hastelloy cylinder with a 2.0 mil niobium-stannide layer, and α of 0.53 was stable throughout the test region; even when the field was applied as rapidly as 500 gauss/second. At this point, it became clear that a more complete investigation of the factors effecting stability of the Nb_3Sn layer, such as rate of field application, thickness of deposit, current density, substrate, geometry of substrate and plating were required. These factors will be discussed in a later section.

b. Multilayered Structures

In parallel with the efforts to obtain stable Nb_3Sn layers, a two-layer cylinder was processed consisting of an initial Nb_3Sn layer 1.1 mils thick and an additional Nb_3Sn layer 1.0 mils thick. Second Nb_3Sn layers were also deposited in thicknesses up to 4 mils thick on Hastelloy and steatite plates (0.75" wide by 1.00" long). A cross section of the latter is shown in Figure 6.

FIG.6 CROSS SECTION OF MULTILAYERED STRUCTURE

Ffom metallographic examination, it is evident that the layers adhered well to each other with no visible void between the layers. Each layer is distinct with a well-defined crystal structure. These results establish the feasibility of assembling such multilayered structures.

c. Factors Influencing Flux Jumps

The magnetic shielding characteristics of a tubular Nb_3Sn layer are strongly influenced by its physical dimensions, testing environment and structure of the Nb_3Sn. These parameters will be discussed below.

(1) Correlation of α with Nb_3Sn Layer Stability

According to the Anderson-Kim description of Type II superconductors, α is a material constant proportional to the current density of the superconductor. The larger the value of α, the more effective are the localized flux pinning sites which provide a rigid matrix against the Lorentz force J x B. When the Lorentz force exceeds the pinning force, flux motion results. The flux motion is more violent in material with a large α, with higher voltages induced, and consequently increased probability of generating flux jumps. Table II presents the effects of increasing α, while maintaining the substrate, rate of field application, film thickness, and diameter essentially constant. It is observed that the instabilities (flux jump frequencies) increase with larger values of α.

TABLE II

Effect of α on Stability of Nb_3Sn Layer

Run No.	Sample	Substrate	Substrate Outside Diameter, Inch	α 10^6kG-Amp. cm^2	Type of Shielding*
28055 #10	11	Steatite	0.250	2.4	Part. Stable
28055 #12	14	Steatite	0.250	5.3	Unstable
28055 #21	23	Hastelloy	0.375	3.4	Part. Stable
28055 #21	22	Hastelloy	0.375	16.6	Unstable
28055 #27	29	Platinum	0.250	1.8	Stable
28055 #29	31	Platinum	0.250	8.9	Stable
28055 #29	30	Platinum	0.250	17.3	Part. Stable

* A stable deposit is one with no flux jumps over the entire region tested. A partially stable deposit is one exhibiting a few flux jumps in the low-field (0-5 kG) region, and an unstable deposit is one exhibiting no stability over the region tested.

(2) Correlation of Nb_3Sn Layer Thickness with Stability

The flux jumping problems associated with thick superconductive layers were mentioned previously. However, even with thin Nb_3Sn layers, differences in stability as a function of deposit thickness were observed. In Table III, two examples of the effects of deposit thickness on stability at essentially the same rate of field application and current density are presented. It became evident that stability decreased with increased film thickness.

TABLE III

Effect of Deposit Thickness on Stability

Run No.	Sample No.	Substrate	Deposit Thickness $\times 10^{-3}$ Inch	Type of Shielding *
28055 #15	16	Steatite	0.7	Part. Stable
28055 #14	18	Steatite	1.3	Unstable
28055 #29	31	Platinum	0.6	Stable
28055 #26	27	Platinum	2.0	Part. Stable

* The definition of stability is the same as described in Table II.

(3) Correlation of Diameter of Nb_3Sn Cylinder with Stability

It has been observed that as the diameter of the Nb_3Sn tube increases, the stability of the deposit decreases. This is shown below in Table IV with a Hastelloy substrate cylinder. In these samples, the rate of field application, deposit thickness and α remain essentially constant. Additional qualitative data relating diameter of the Nb_3Sn deposit with stability has been described but in these cases, the comparison is not clear cut since the deposit thickness, α, and substrate were not identical.

TABLE IV

Effect Diameter on Nb_3Sn Layer Stability

Run No.	Sample No.	Substrate	Substrate O.D., In.	Type of Shielding *
28055 #19	21	Hastelloy	0.250	Stable
28055 #21	23	Hastelloy	0.375	Stable
28055 #24	25	Hastelloy	0.500	Part. Stable

* The definition of stability is the same as used in Table I.

(4) Effect of Rate of Field Application on Stability of Nb_3Sn Layer

The stability of the Nb_3Sn layer is strongly influenced by the rate of field application, i.e., higher rates of field application increase frequency of flux jumps. This effect is shown in Figures 7 and 8, where the rates of field application on the same cylinders are increased from 8 to 20 gauss/sec. Similar rate dependence follows naturally from the Anderson-Kim analysis in that with a higher rate of field application, the flux bundles build up rapidly at particular sites and exceed the relaxation rate of the flux bundles in the superconductor. This causes more frequent flux jumps.

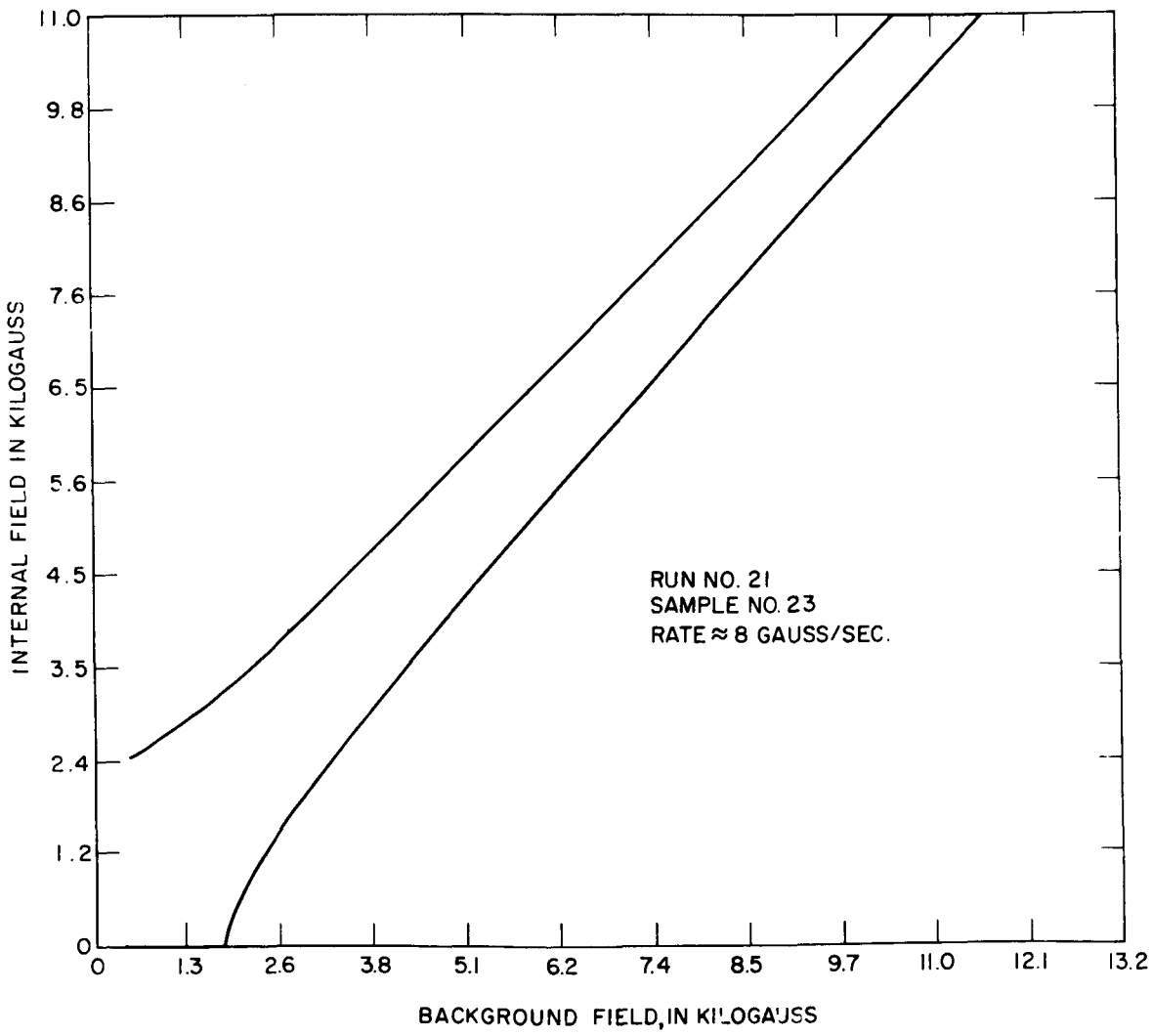

FIG. 7 CRITICAL STATE CURVE WITH FIELD APPLIED AT 8 GAUSS / SECOND

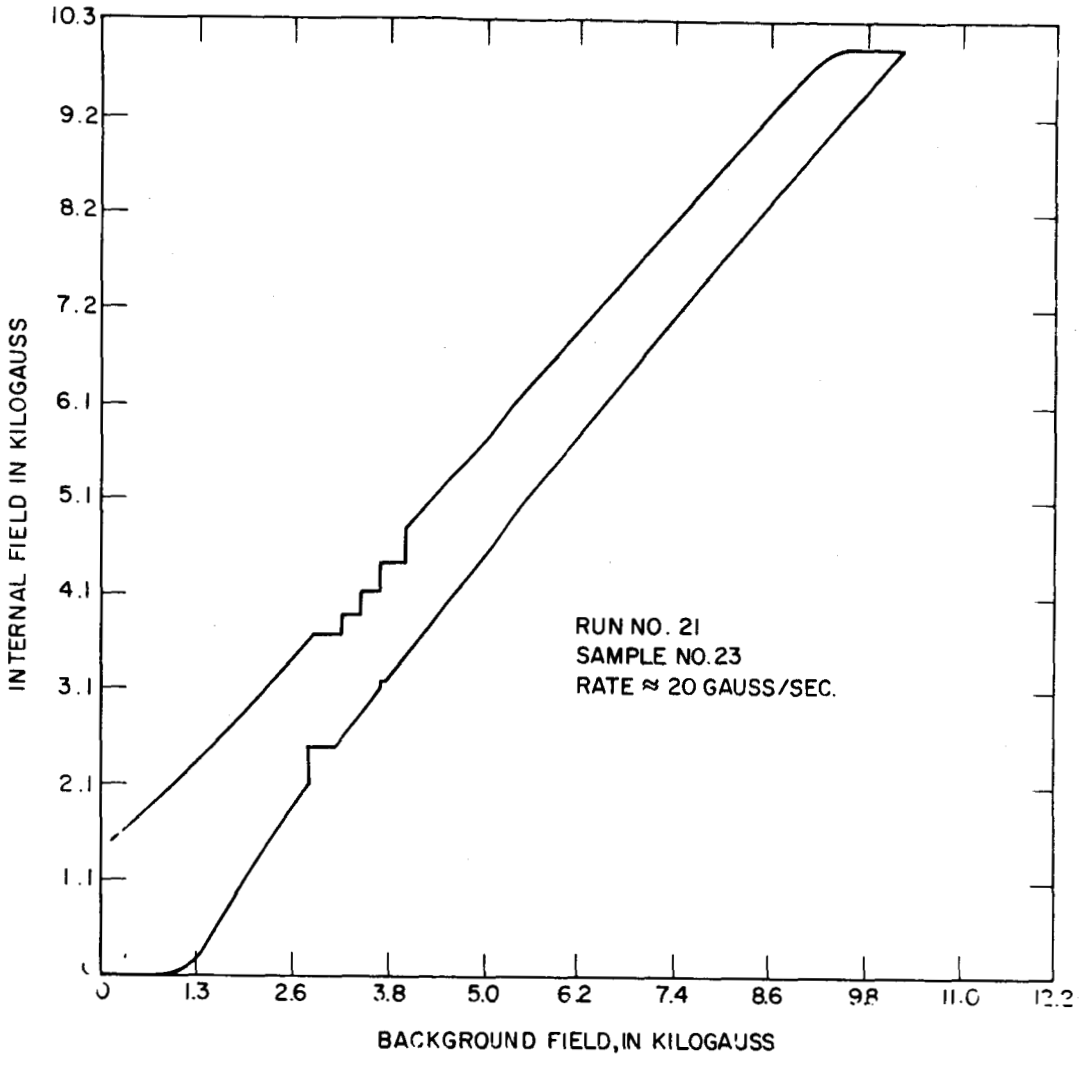

FIG.8 CRITICAL STATE CURVE WITH FIELD APPLIED AT 20GAUSS/SECOND

(5) Effect of Substrate on Stability of Nb_3Sn Layer

The substrate on which the Nb_3Sn layer is deposited effects the orientation and growth rate of the Nb_3Sn layer in addition to which it can also act as an energy sink. Difference in stability between platinum and steatite cylinders, with approximately the same Nb_3Sn deposit thickness, current density, rate of field application and diameter are shown in Figures 9 and 10.

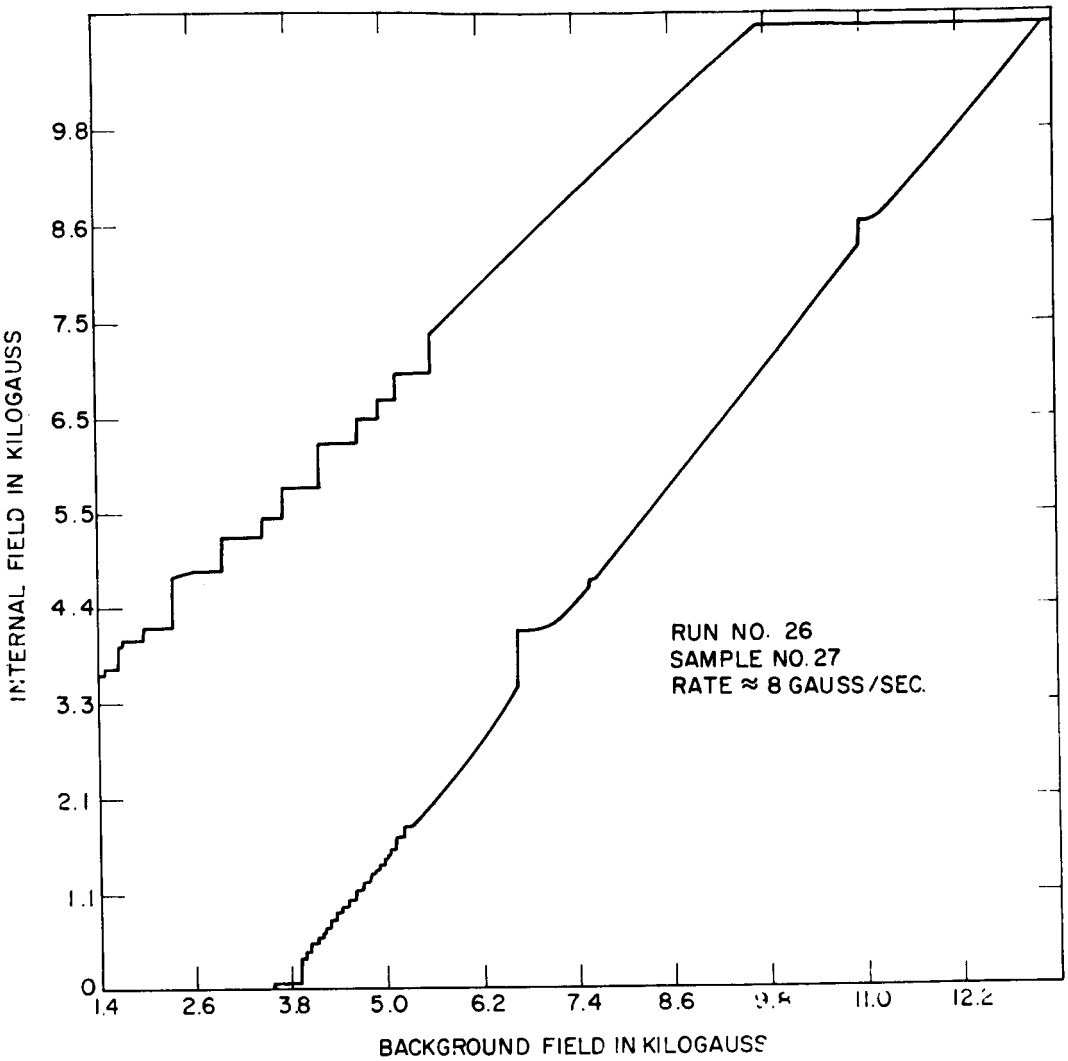

FIG. 9 CRITICAL STATE CURVE OF Nb_3Sn DEPOSIT ON PLATINUM SUBSTRATE

Although both cylinders are unstable, the flux jumps with the platinum substrate cylinders are narrower, shielding a portion of the field at all times and indicating that only a localized portion of the coating on the cylinders becomes normal. When a flux jump occurred in the Nb_3Sn on the steatite substrate, the entire cylinder became normal so that the entire background field penetrated the cylinder. Applied field rate in both cases was 8 gauss/second. The improved stability is attributed to the superior electrical and thermal conductivity of the platinum substrate,

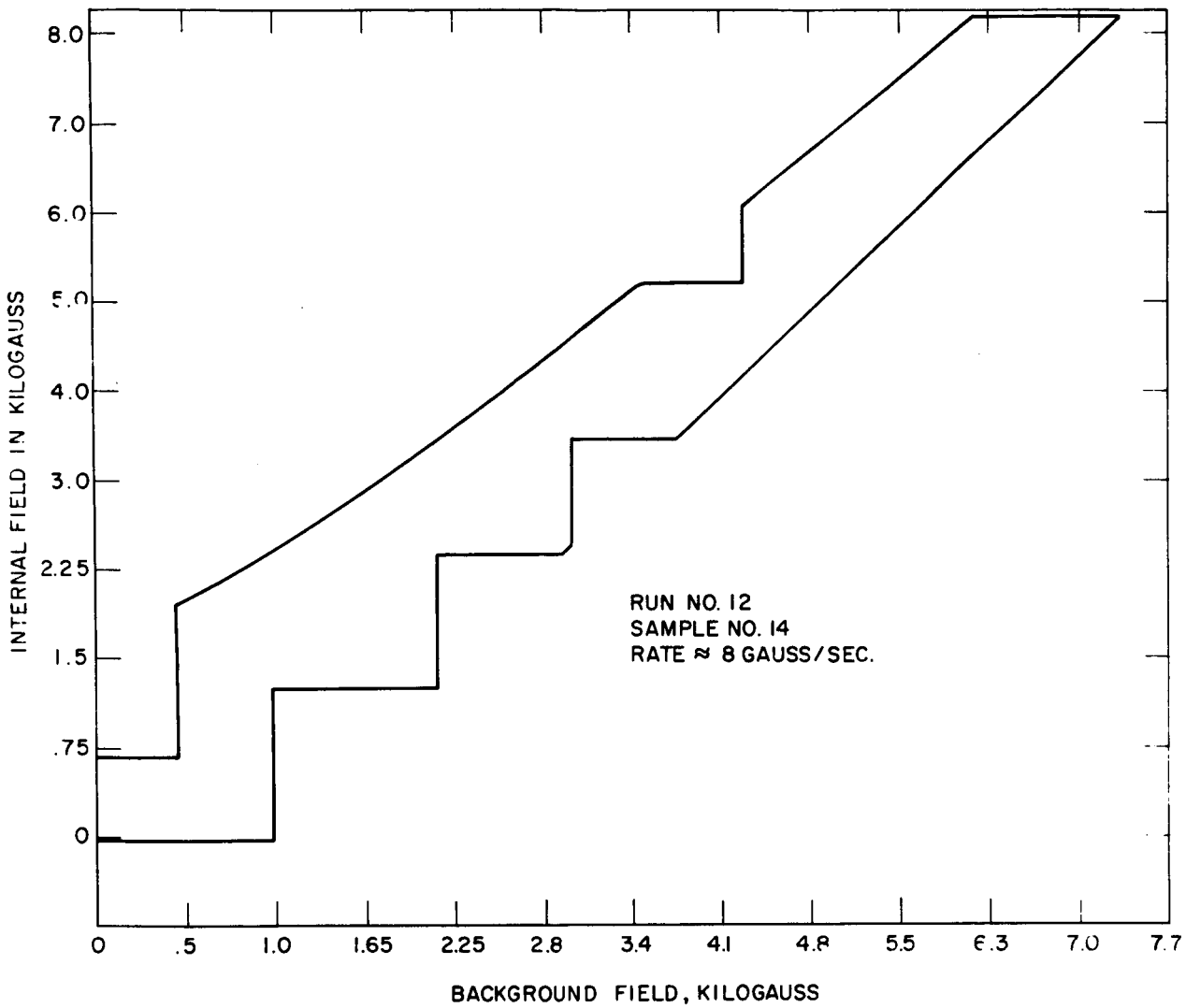

FIG.10 CRITICAL STATE CURVE OF Nb_3Sn DEPOSIT ON STEATITE SUBSTRATE

(6) Effect of Plating on Stability of Nb_3Sn Layer

To stabilize the thin Nb_3Sn layer, a plated coating of silver was applied. The silver plating acts both as an eddy current and shunting current sink, and also as a thermal conductor for energy released during flux movement. The quality of the silverplate in terms of purity and crystal structure affects both the electrical and thermal conductivities of the coating. A decrease in lattice defects and impurities will increase both the thermal and electrical conductivities. The highest degree of stabilization is obtained with silver coating having the highest electrical and thermal conductivities. Figures 11, 12, and 13 show the shielding behavior of cylinder 28055-24 No. 25 under the following conditions: (1) initially unplated, (2) silver plated at 33 amperes/foot^2, and (3) the silver plating removed and replated at 5 amperes/foot^2. A larger crystal structure is obtained with slower plating rates. It is inferred that the silver plating stabilizes the Nb_3Sn layer to a degree; and whereas partially stable deposits can be converted to completely stable deposits, initially unstable deposits cannot be completely stabilized. No changes in current density of the Nb_3Sn layer were observed as a result of silver plating.

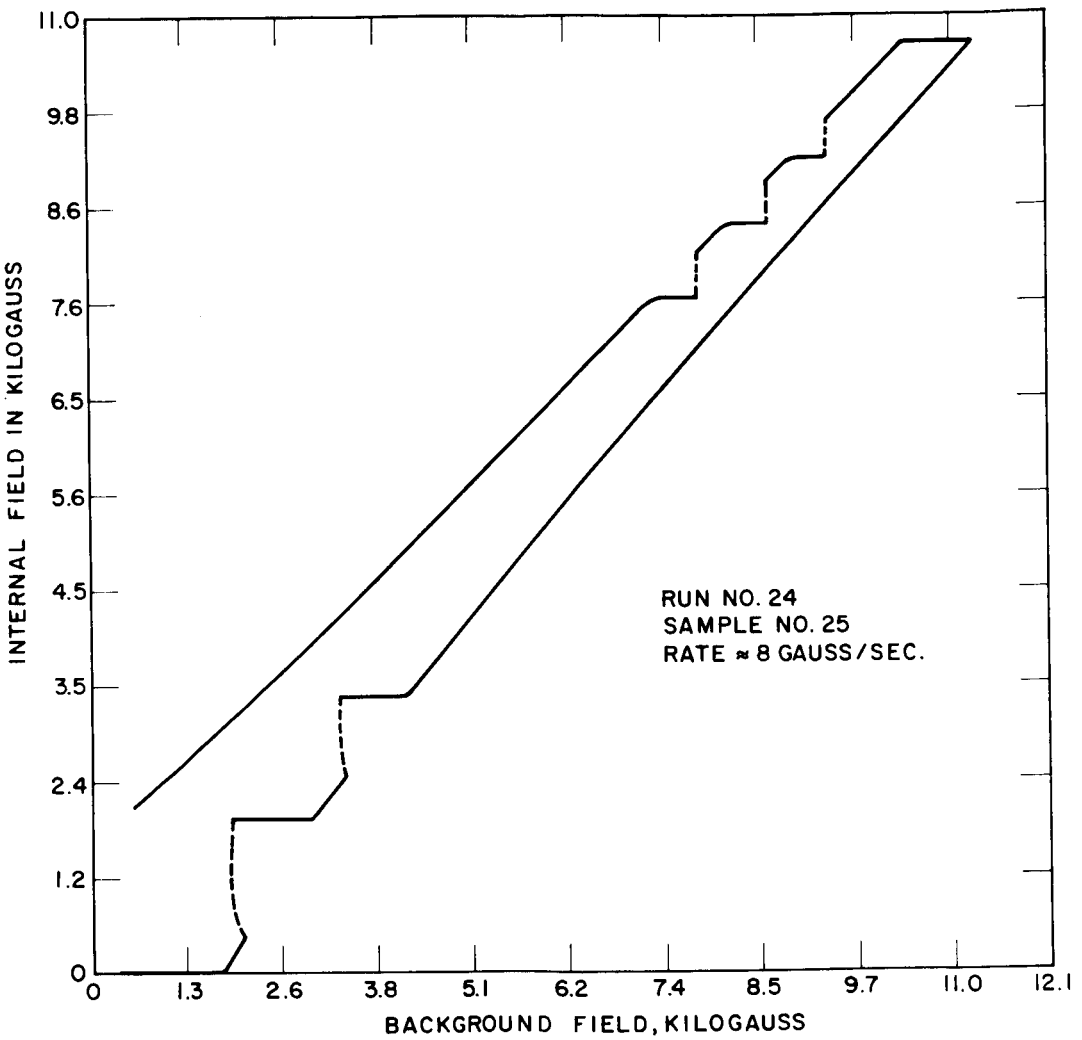

FIG. 11 CRITICAL STATE CURVE, UNPLATED

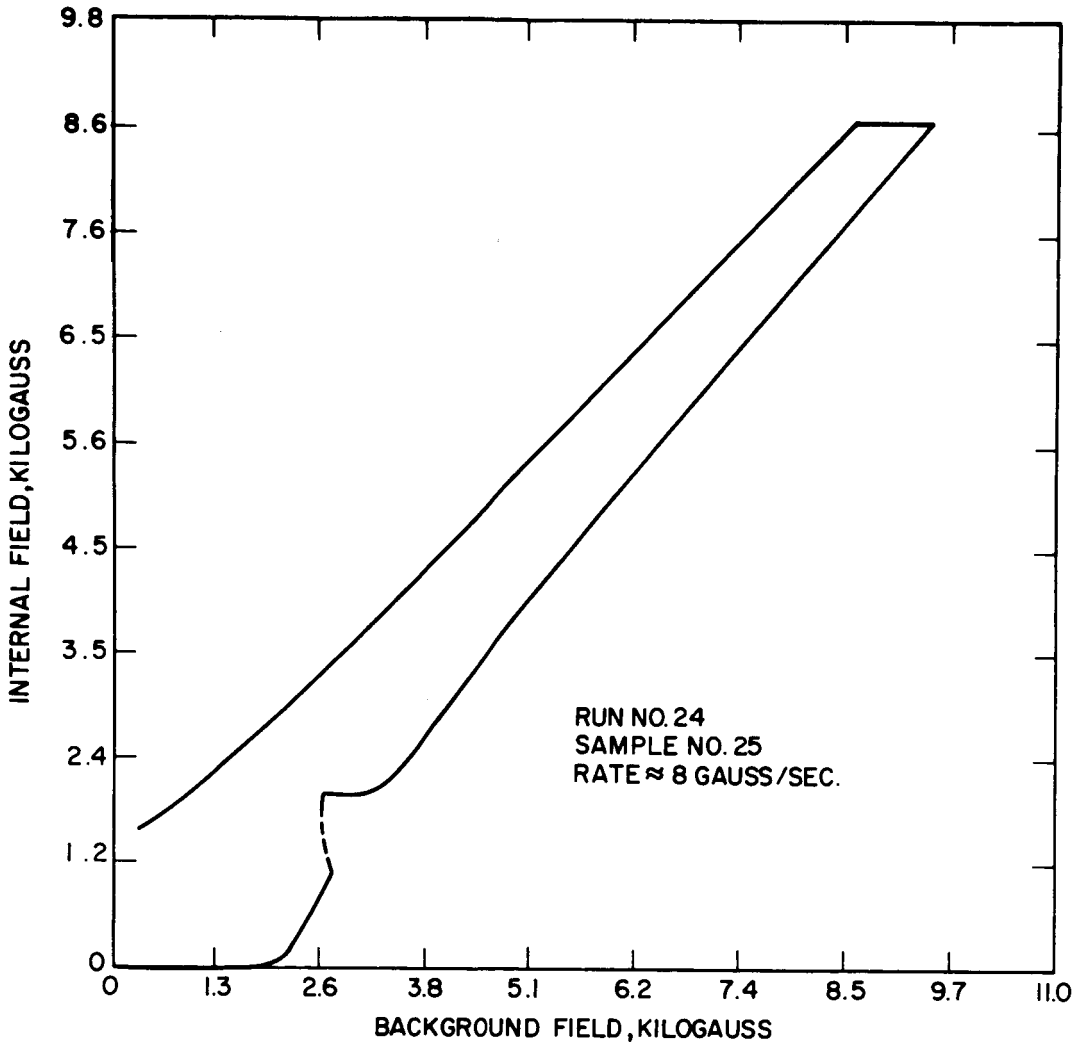

FIG. 12 CRITICAL STATE CURVE AFTER SILVER PLATE AT 33 AMPERES / ft^2

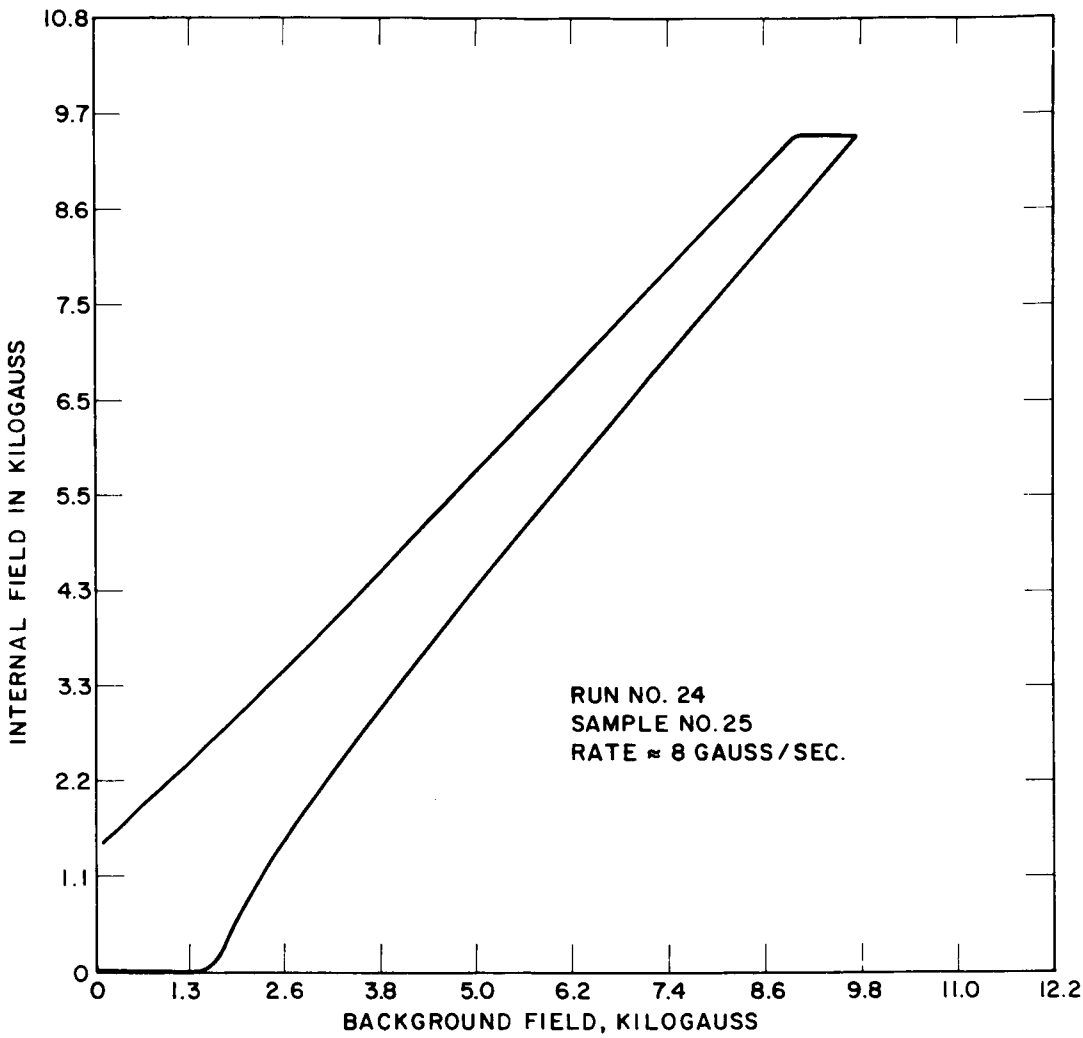

FIG.13 CRITICAL STATE CURVE AFTER SILVER PLATE AT 5 AMPERES/ft.^{2}

(7) Correlation of Experimental Results with Present Theory

The experimental results discussed above are in apparent agreement with recent calculations of Wischmeyer and Kim[9]. In hard superconductors, as flux lines, pinned to structural defects, creep by Lorentz forces and thermal activation power is dissipated. With increased power dissipation, flux creep can turn into turbulent flow, causing catastrophic breakdown of flux structure here described as a flux jump.

The onset of a flux jump occurs at a critical power level. The expression for power dissipation is $P = J \cdot E \cdot A \cdot$, where J is the current density, E is the induced voltage, and A is the conductor area. Substituting $J = \alpha/(B_o + H)$, where α is a material constant, B_o is a constant, and H is the applied field, $E = 10^{-8}\pi a^2$ where πa^2 is the cross section area of the shielded area, and assuming a conductor cross section area equal to the Nb_3Sn layer thickness and unit length, one obtains the expression for power dissipation:

$$P = \frac{\alpha}{B_o + H} \quad 10^{-8} \quad \pi a^2 \quad \frac{dH}{dt} \quad w \qquad (11)$$

On the basis of power dissipation per unit surface area of superconductor, the expression becomes:

$$Q_{dis} = \frac{\alpha}{B_o + H} \quad 10^{-8} \quad \pi a^2 \quad \frac{dH}{dt} \quad w \, \frac{1}{2\pi a} \qquad (12)$$

or:

$$Q_{dis} = 10^{-8} \quad \frac{aw}{2} \quad \frac{\alpha}{B_o + H} \quad \frac{dH}{dt} \qquad (13)$$

if $B_o << H$, then (3) becomes:

$$Q_{dis} = 10^{-8} \quad \frac{aw}{2} \quad \frac{\alpha}{H} \quad \frac{dH}{dt} \qquad (14)$$

where: a = radius
w = wall thickness
H = background field
$\frac{dH}{dt}$ = rate of field application
α = material constant

Since the onset of flux jumps occurs at a critical power level, any variable in (4) which tends to increase the power dissipation will also increase the frequency of flux jumps. Thus, one expects that the frequency of flux jumps should increase as (1) α increases, (2) Nb_3Sn layer thickness increases, (3) radius increases, (4) $\frac{dH}{dt}$ increases and (5) H decreases.

The critical power level of a thin deposit can also be altered by changing the thermal and electrical environment. If the substrate and metal plating is a good thermal conductor, local heating within the superconductor resulting from flux motion can be rapidly dissipated and consequently the catastrophic breakdown of the flux structure will occur at a higher power level than if the thermal sink were not present. Similarly, a good electrical conductor acts as a current shunt for a local portion of the superconductor reverting to the normal state.

The variation of the above parameters are:

Parameter	Variation
α	1 to 18 x 10^6 kG-amp/cm^2
Thickness of Deposit	0.6 to 2 x 10^{-3} inches
Diameter of Cylinders	0.250 to 0.500 inches
Rate of Field Application	8 to 20 gauss/sec.
Background Field, kG	0 to 12 kilogauss
Conductivity of Substrate	1 x 10^{-3} to 1 x 10 watt/cm^{o} K

The largest variation of the parameters is observed in the conductivity of the substrate. The energy removed from the Nb_3Sn substrate interface through the substrate is given by:

$$Q_{removed} = kS \frac{\Delta T}{\Delta L} \qquad (15)$$

Where: Q - energy removed through substrate per unit area per unit time
k - thermal conductivity
S - surface area
$\Delta T/\Delta L$ - temperature gradient

This is, however somewhat misleading since any energy generated within the Nb_3Sn must be removed through the Nb_3Sn layer to reach the substrate. The conductivity of the Nb_3Sn at 4^oK is relatively poor and consequently it is the Nb_3Sn that is the thermal dissipating barrier. It is, therefore, very difficult to access the relative importance of the substrate and the other above discussed parameters in terms of primary versus secondary factors.

The theoretical considerations discussed above are in general agreement with the observed experimental results.

IV. DEPOSITION OF Nb_3Sn ON TWO-INCH WIDE RIBBON

A. INTRODUCTION

It had been generally supposed that the shielding of high magnetic fields in large volumes requires either thick Nb_3Sn deposits or multilayered structures consisting of alternate thin layers of Nb_3Sn and a normal conductor. Based on the experimental evidence and theoretical considerations presented in Section III, it is not yet evident that shielding high magnetic fields by thick deposits or multilayered structures free from flux jumps in large diameter cylinders will be feasible.

An improved approach for shielding high magnetic fields free from flux jumps consists of stacking discs with concentric rings of silver-plated niobium-stannide[10]. A schematic representation is shown in Figure 14. This construction permits a separation of Nb_3Sn rings and based on cross sectional area, limits the induced total shielding current per ring. In the event that a superconductive ring reverts to the normal state, the remaining rings of the stack on the same or adjacent discs are not effected since the rings are

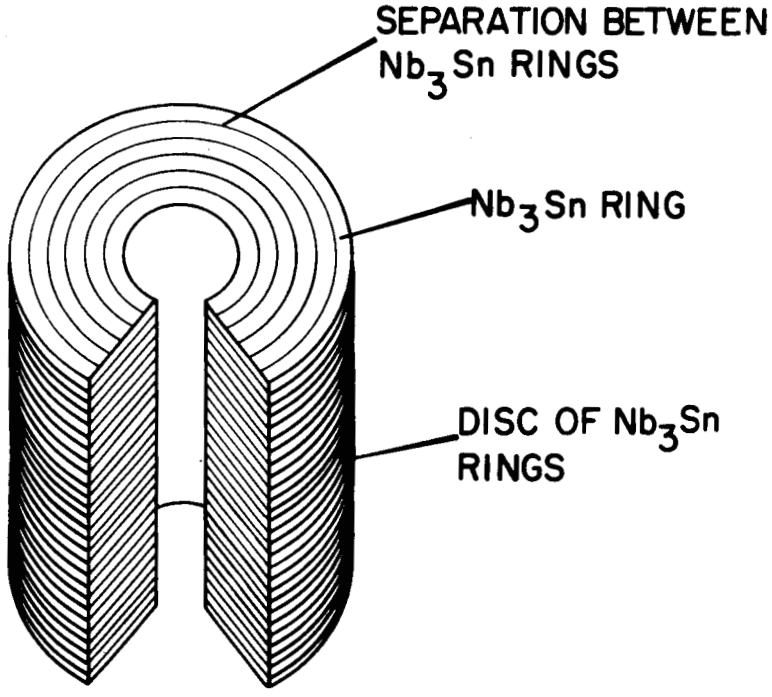

FIG. 14 STACKED DISC, CONCENTRIC Nb_3Sn RING, MAGNETIC SHIELD

insulated from each other. This principle permits the construction of an extremely stable shielding device. The feasibility of this approach was demonstrated by J. J. Hanak[4] using a 0.2-inch bore magnet stack.

Scaling factors for large volumes were evaluated by assembling a ½-inch inside diameter and 1-7/8-inch outside diameter shielding device. This approach should be equally well adaptable to flux concentration, energy storage devices and flux pumps. The discs are punched from a 2-inch wide ribbon coated with Nb_3Sn. A description of the deposition apparatus for coating the 2-inch wide ribbon, processing of the discs, and electromagnetic characteristics are presented in the following sections.

B. PROCESS

1. Deposition of Nb_3Sn on 2-Inch Wide Ribbon

In principle, the vapor-deposition process for depositing Nb_3Sn on a continuously moving 2-inch wide ribbon 0.0005-inch thick is the same as that employed for deposition on cylinders and flats. The mixed chlorides of niobium and tin are volatilized and transported to a deposition zone where they are reduced by hydrogen to form a continuous deposit of interlocking Nb_3Sn crystals. An exploded view of quartz apparatus for depositing Nb_3Sn continuously on 2-inch wide ribbon is shown in Figure 15.

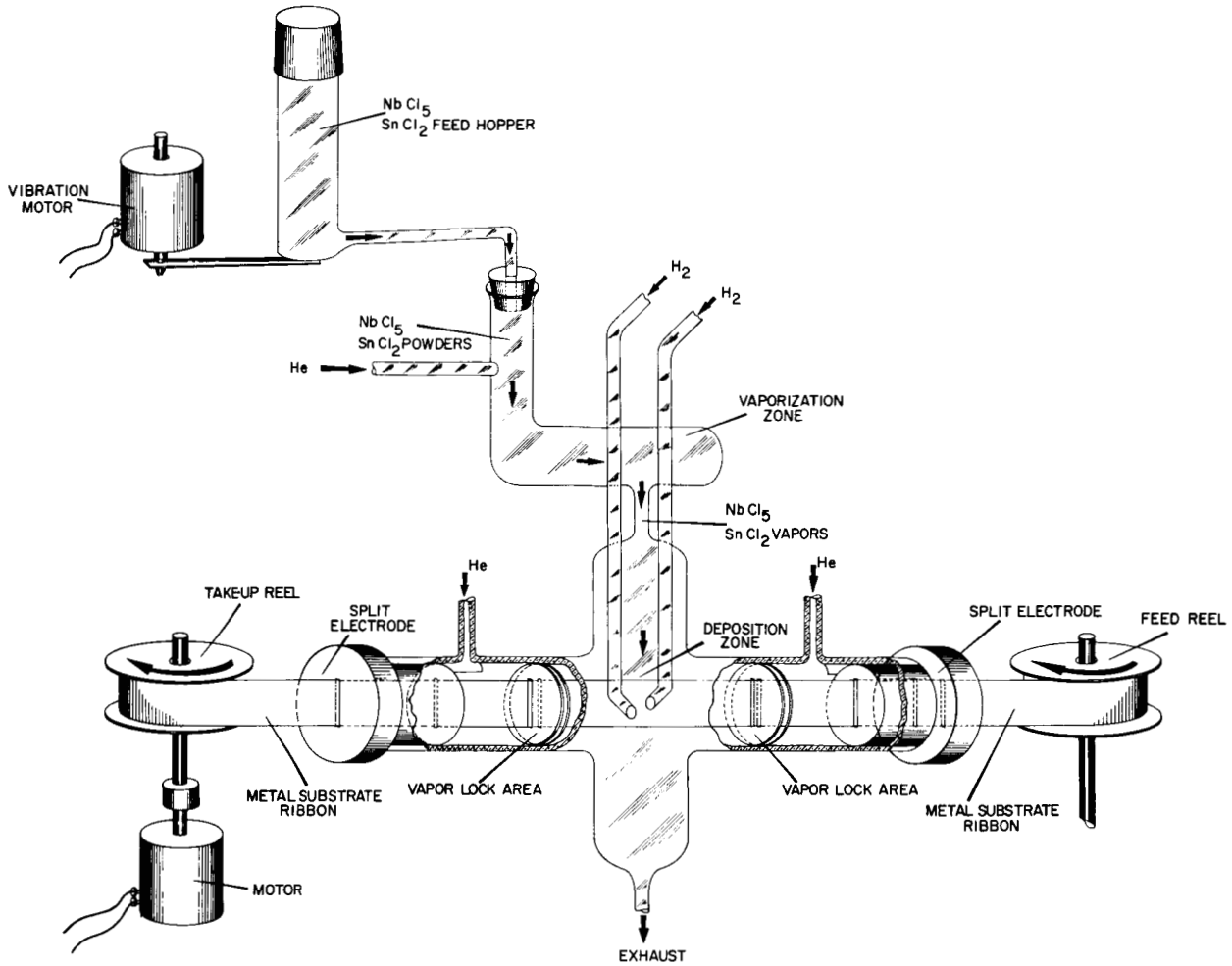

FIG. 15 Nb_3Sn WIDE RIBBON DEPOSITION APPARATUS

2. Operation of Apparatus

Mixed powders of niobium-pentachloride ($NbCl_5$) and tin-dichloride ($SnCl_2$) are metered into the system by the vibratory action imposed on a feed hopper. The solid chlorides drop into a high temperature volatilization chamber where they are vaporized. The mixed $NbCl_5$ and $SnCl_2$ vapors then pass through a narrow restriction into the deposition chamber. This restriction between the volatilization and deposition zones minimizes back flow of vapors from the deposition chamber. A positive flow of helium introduced into vaporization chamber prevents back flow of chloride vapors into the feed system and provides additional velocity to the metal chlorides entering the deposition zone.

In order to maximize turbulence, a strong flow of H_2 is introduced horizontally into the deposition chamber. The hydrogen flow is at right angles to both the ribbon travel and the downward flow of the helium, metal-chloride-vapor mixture. Unreacted gases and reaction products are exhausted at the bottom of the apparatus.

The actual metal chloride utilization in the deposition process is approximately 20%. The chloride utilization is kept low so that a high concentration of unreacted chlorides continuously surrounds the moving ribbon and the hydrogen reduction is not diffusion limited.

The moving ribbon enters and leaves the apparatus through a multiple-point electrode contact Figures 16 and 16A. A vapor-lock area between the carbon electrodes and deposition zone prevents the deposition of metal chlorides on the electrodes. The ribbon is resistance heated above the furnace wall temperature. The vapor lock consists of an insert assembly having two slotted discs through which the ribbon passes. Helium is injected into both outer insert assemblies. The helium flowing into the narrow restriction between the ribbon and the wall of the two slots in series contain the chlorides in the deposition zone. This is shown in Figure 15.

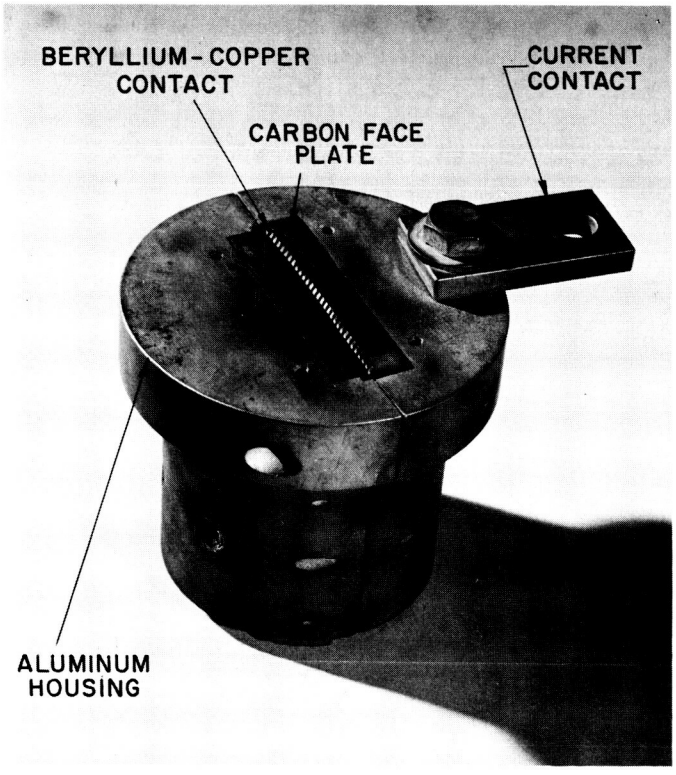

FIG. 16 ASSEMBLED, MULTIPLE POINT ELECTRODE CONTACT

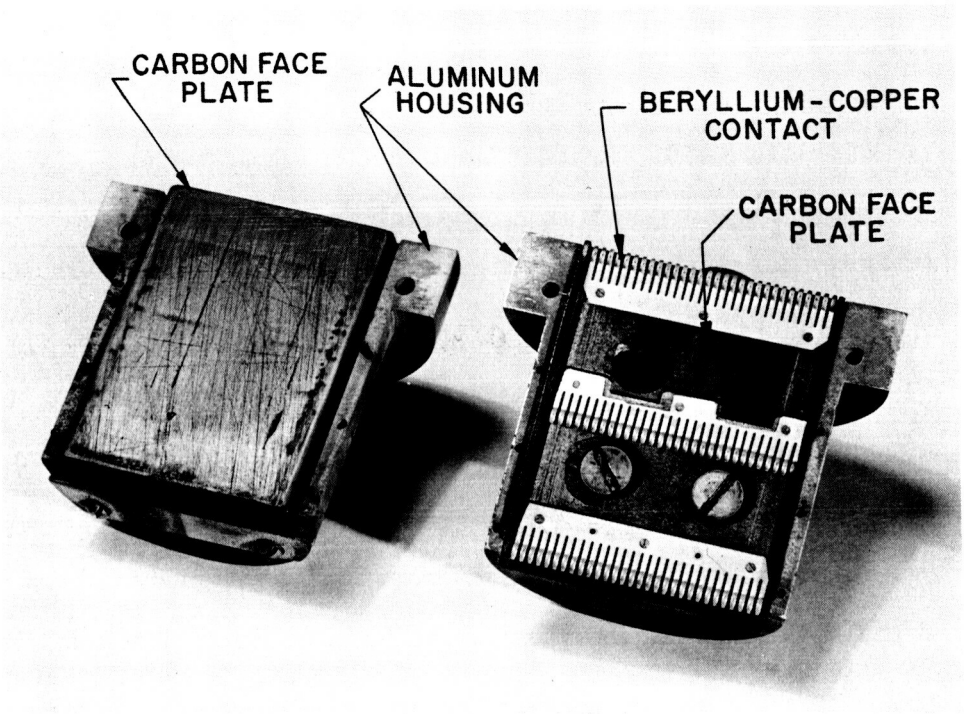

FIG. 16A DISASSEMBLED, MULTIPLE POINT ELECTRODE CONTACT

A typical set of operating conditions is listed below:

(1)	Temperature	Volatilization Champer	640°C
		Deposition Zone	730°C
		Ribbon	900°C
(2)	Gas Flows	$NbCl_5$	0.28 mole/hour
		$SnCl_2$	0.28 mole/hour
		Hydrogen	3.5 mole/hour
		Helium	2.2 mole/hour
(3)	Ribbon Speed		2 meters/hour

Experimental runs were made to test the design of the wide ribbon apparatus and all of its components. Operating conditions of gas flow and temperature were established and sufficient ribbon was processed to build a stack of concentric Nb_3Sn disc.

The length of test runs varied from two to twelve meters. A compilation of these runs are listed in Table V.

TABLE V - Deposition Conditions and Evaluation of the 2 inch Ribbon

Run #	Principle Design Parameters	Ribbon Position	Process Conditions: Atomic Ratio Nb/Sn	Process Conditions: $NbCl_5$+$SnCl_2$ Feed Rate gm/hr	Process Conditions: Temperature Deposition Zone °C	Process Conditions: Volitalization Zone	Process Conditions: Ribbon Current, amps	Process Conditions: Ribbon Speed meters/hr	Chemical Analysis % Nb: Top side	Chemical Analysis % Nb: Bottom side	X-Ray Results	Current Density amps/cm^2	Observations
WR 1	Diffusion plate separating volatalization and deposition zones Carbon plate electrodes	Ver.	1/1		775	775	20	1			Nb_2Sn + Nb_3Ni	$1.8x10^5$	Deposit was streaked and discolored. Heavy metal deposit above diffuser plate indicated that substantial chlorides were stripped from gas stream before reaching deposition zone.
2	"	Ver.	1/1		775	775	20	1			"	Resistive	
3	"	Ver.	1/1		800	800	25	1			"	Resistive	
4	(same as 1)	Ver.	1/1		700	700	25	1.3			Nb_3Sn		Deposit streaked and discolored At 500 & 600°C heavy condensation of chlorides occurred in volatilization zone.
5	(same as 1)	Ver.	1/1		600	600	25	1.3			"		
6	(same as 1)	Ver.	1/1		550	550	25	1.3	76.3	76.7	5.231Å	$1.8x10^5$	
7	Replacement of diffusion plate with a volatilization chamber separated from the deposition zone by a tubular restriction.	Ver.	1/1	60	650	620	20	1.3	76.0	76.3	Nb_3Sn	$1.2x10^5$ 5.235Å	Streaking reduced somewhat with higher feed rates. Runs 1 through 9 had severe electrical arcing through ribbon. Wrinkle type deformation on ribbon due to uneven distribution of pressure inside the electrodes.
8	Rearrangement of heating elements into 2 zone control			60+	650	640	25	1.3				$1.5x10^5$	
9	(same as 8)		1/1	60+	710	670	25	1.3	75.6	75.8			
10	Ribbon positioned horizontally	Hor.	1/1	75	650	620	25	1.3	76.1	74.9	Nb_3Sn 5.298Å	Resistive	Intermittant streaking of deposit. Metal deposits in volitalization zone. No electrical arcing. Uniform deformation ribbon causing coiling.
11	Water cooled mercury electrode same as 10	Hor.	1/1		710	680	25	1.3	76.3	75.1		$5.9x10^4$	
12	Same as 10	Hor.	1/1	80	720	710	30	1.3	77.0	75.8	"	$4.7x10^4$	
13	Same as 10	Hor.	1/1	75	735	710	40	1.3	76.8	75.7	"	30-25-2	
14	(same as 7-9) plus Ribbon repositioned vertically	Ver.	1/1	85	710	690	25	1.3	76.8	75.7	Nb_3Sn 5.231Å	$5.9x10^5$	Streaking of ribbon reduced by higher chloride feed rate.
15	Multiple contact electrode, 1st design same as 14	Ver.	1/1	90	715	680	25	1.3				$8.8x10^5$ $8x10^5$ 160-25	Some arcing and some wrinkling
16	Same as 14[5]	Ver.	1/1	90	710	690	25	1.3	75.5				
17	Furnace rebuilt to provide insulation between deposition a volitalization zones. Temperature of each zone was controlled.	Ver.	1/1	120	715	680	25	1.5	76.1	76.4	Nb_3Sn 5.235Å	$1.5x10^5$	Nb_3Sn deposit is metallic in appearance without any streaking. This is due to a sharp increase in chloride feed rate Some arcing.
18	Same as 17 plus improved multiple contact point electrode	Ver.	1/1	130	730	660	25	1.5	75.7		Nb_3Sn 5.233Å	$1.1x10^5$	Infrequent arcing. Some ribbon deformation.
19	Same as 18		1/1	160	730	650	25	2	76.0			$1.7x10^5$	
20	Tabulation provided for H_2 pulsing	Ver.	1/1	150	730	650	30	2	75.3		Nb_3Sn 5.230Å	$1.7x10^5$	Infrequent arcing Deformation minimized by increased gas turbulence within deposition zone.
21	Same as 20	Ver.	1/1	130	740	650	30	2	75.9			$1.7x10^5$	

In the first few experimental runs major emphasis was placed on the design and assembly of the deposition equipment. X-ray analysis of these runs indicate variations of the lattice constant and the presence of a second phase. In latter runs attainment of compositional stoichiometry was emphasized, and in these runs the deposits on the Nb_3Sn layer were a β-tungsten structure, single phase, with lattice constant of 5.290°A and 5.230°A. These values are somewhat different from the lattice constants of 5.290°A for Nb_3Sn on flats and cylinders. These differences can be attributed to (1) stress of the Nb_3Sn layer due to the differences of coefficient of expansion between the very thin (0.5×10^{-3} inch) substrate and Nb_3Sn and (2) compositional variations which were not detected as a second phase.

3. Design Factors

a. The first apparatus was constructed with a diffuser plate between the volatilization and deposition chamber. The diffuser plate was circular with radial .040-inch slots at approximately 22^{o} intervals. Hydrogen was introduced above the diffuser plate where it mixed with the metal chloride vapors. Heavy Nb_3Sn deposits formed on the diffuser plate during the operation of the apparatus resulting in a constriction of the slots.

The volatilization and deposition zones were subsequently physically separated into two zones controlled at different temperatures. Maintaining the volatilization zone at a lower temperature than the deposition zone minimizes the premature partial reduction of chlorides to a non-volatile form before reaching the deposition zone.

b. It was found necessary to position the moving ribbon in the vertical plane to minimize deformation of the Nb_3Sn-coated ribbon. The orientation of the ribbon with respect to the reacting gases aided in obtaining a uniform Nb_3Sn deposit composition and thickness from side to side. When the alignment of the ribbon was maintained horizontal, a slight sag was produced in the ribbon while at the high reaction temperature and this deformation became permanently set after the deposition of Nb_3Sn. The horizontal positioning of the ribbon also created a problem with respect to gas mixing. The effect of gravity on gases having widely different densities made difficult thorough and adequate mixing over the distance between their introduction point and the deposition area. The effect of the horizontal gas flow is shown by the observed difference in chemical composition and the deposit thickness between the two sides of the ribbon.

c. Multiple contact electrodes - The most effective contact for vertically positioning the ribbon was found to be a spring-loaded carbon brush electrode containing multiple beryllium-copper contact points. This contact conducted 40 amperes to the moving ribbon without arcing or oxidation (Figures 16 and 16A).

d. A water-cooled mercury contact designed for the horizontally positioned ribbon was found satisfactory. This contact is shown in Figure 17.

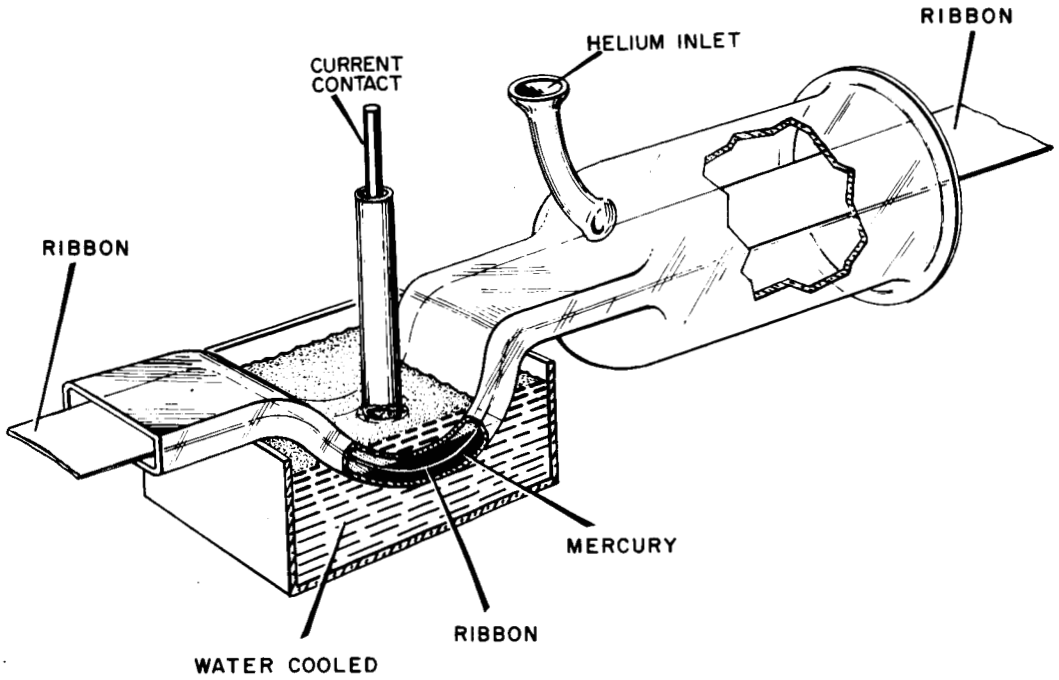

FIG. 17 HORIZONTAL CONTACT

e. Removable vapor lock inserts - The inserts provide a vapor lock confining the vapors in the deposition zone and isolating the reactants from the electrode area. The insert can be removed while the apparatus is hot in order to thread the ribbon through the apparatus without disassembly. The inserts are shown in Figure 15 as part of the entire apparatus.

C. CONCENTRIC RING PATTERN PROCESSING

Conventional photoresist and chemical techniques were employed to etch out Nb_3Sn concentric ring patterns from the 2-inch wide Nb_3Sn-coated Hastelloy ribbon.

Fourteen-inch lengths of niobium-stannide coated Hastelloy ribbon are cut from the continuous 2-inch wide ribbon to permit batch silver plating. A thin nickel flash coating is initially applied to the Nb_3Sn to improve the adherence of the silver plating. No attempts were made to determine the effect, if any, of the ferromagnetism associated with this nickel coating. The silver is plated at a current density of 33 amperes/foot^2 in a standard silver-cyanide plating bath to a coating thickness of 0.2 to 0.3 mils. This plated silver coating adheres well to the niobium-stannide and is adequate for protecting the Nb_3Sn during subsequent chemical etching steps.

The photoresist pattern is applied by standard recommended procedures of the Kodak Company as follows:

1. Dip the silver-plated strip in Kodak Metal Etch Resist (KMER).

2. Prebake the coated strip at 50°C for ten minutes.

3. Insert the 2-inch tape in the exposure fixture (Figure 18).

4. Expose the ring pattern on both sides on the tape using a point source mercury light.

5. Dissolve the unexposed KMER in hot water.

6. Postbake the strip at 130°C for 20 minutes to harden the exposed KMER.

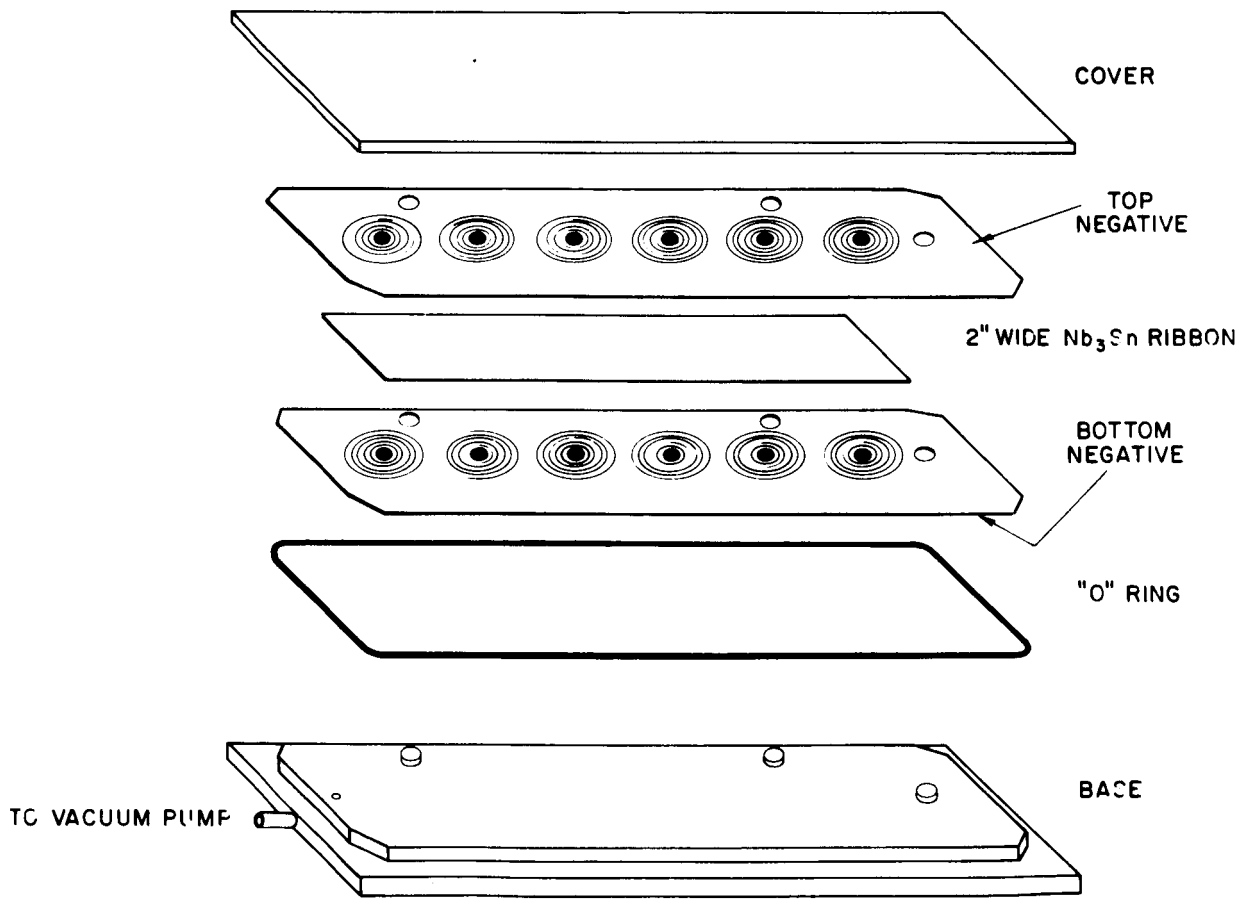

FIG. 18 2" RIBBON EXPOSURE FRAME

The now unprotected silver areas are dissolved out in a room temperature ferric nitrate solution. The exposed niobium-stannide is then removed by chemically etching in a hot (90 to 100°C) caustic KOH solution. The masked region is not attacked since both the KMER and silver are both chemically resistant to the KOH etch solution. The finished discs are then either stamped in a compound punch or chemically etched out from the 2-inch wide ribbon. In chemical etching, the center rings of the bare Hastelloy are masked, leaving only a disc. A cross-section of the disc is shown in Figure 19. Figure 20 demonstrates the progression of steps for processing the concentric ring pattern.

The disc yield from the first few 14-inch long, 2-inch wide strips was only 50 percent. However, after alleviating most minor photoengraving and chemical processing difficulties, the over-all yield was increased to over 95 percent. The photoengraving and chemical etching techniques developed for the discs are also applicable to other intricate device fabrication requirements. Some of these devices will be discussed in Section VI.

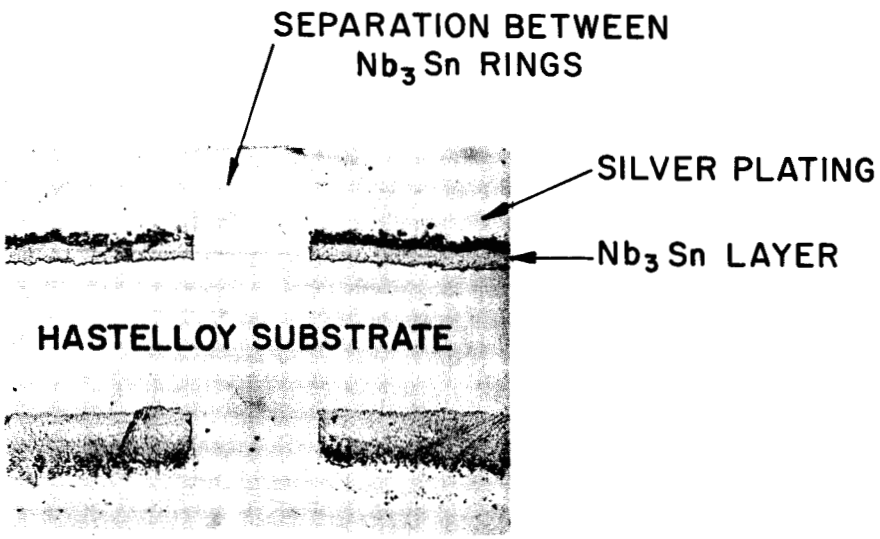

FIG. 19 CROSS SECTION OF A PORTION OF A DISC

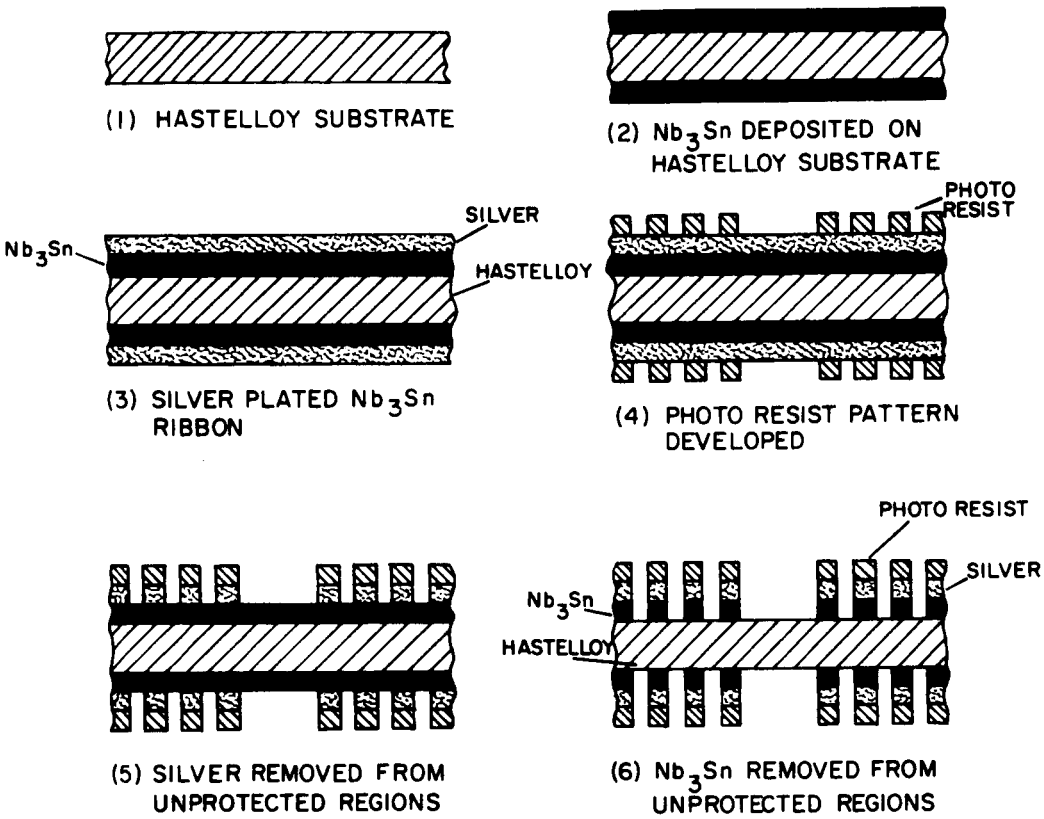

FIG.20 PROCESSING OF CONCENTRIC RING PATTERN

D. SHIELDING BEHAVIOR OF ARBITRARILY SHAPED CYLINDERS

The shielding characteristics of an arbitrarily shaped cylinder can be characterized in terms of α and B_o of the Nb_3Sn ribbon. Rearranging equation III-B-5 gives:

$$H' - H = k\ w\ j = M \tag{16}$$

where M, the magnetization, is the difference between the internally measured shielded field and the externally applied field. The H/I of cylinder can be calculated according to accepted techniques[11]. Incorporating this into the above expression gives:

$$M = H' - H = k\ w\ j = \frac{H}{I\ (B)} \cdot I\ (B) \tag{17}$$

If to a zero order approximation the same average current per ring for the entire cylinder (disc stack) is assumed, expression (17) becomes:

$$k\ w\ j = \frac{H}{I} \cdot I = \frac{H}{I}\ .\ j\ A \tag{18}$$

or:

$$k\ w = \frac{H}{I}\ .\ \ A = \frac{H}{I}\ .\ wt$$

where A is the average conductor cross section area equal to the thickness of the disc multiplied by the average width per ring. Substituting equation (17) into (18) and writing g for $\frac{H}{I}$, and $\frac{\alpha}{B_o + H}$ for j gives:

$$k\ w\ j = \frac{H}{I}\ \ wt\ \frac{\alpha}{B_o + H} = g\ w\ t\ \frac{\alpha}{B_o + H} = M \tag{19}$$

or:

$$\alpha\ g\ w\ t = M\ (B_o + H) \tag{20}$$

or:

$$\frac{1}{M} = \frac{1}{gwt}\ (B_o + H) \tag{21}$$

Thus, an experimental plot of $\frac{1}{M}$ vs. H allows us to evaluate the average values for the constant α and B_o for the entire cylinder.

E. EXPERIMENTAL RESULTS

A 2-1/8-inch inside diameter by 4.5-inch outside diameter by 2¼ inches long, 30-kilogauss magnet was assembled to provide a background magnetic field for determining the shielding characteristics of various disc stack arrays. The test magnet and disc array mounted on the testing holder are shown in Figures 21 and 21A.

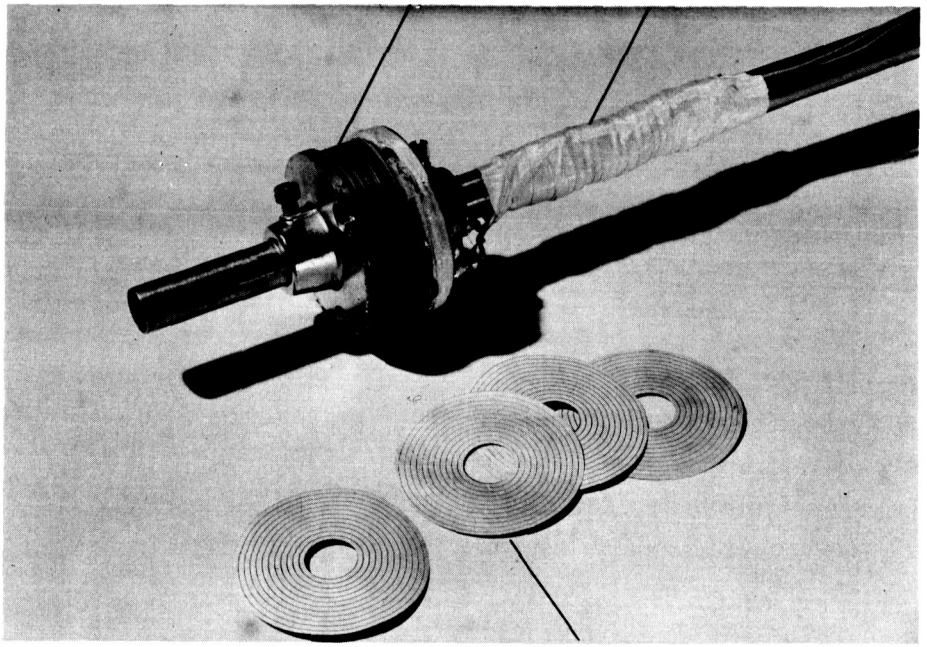

FIG. 21 DISCS AND ASSEMBLED CONCENTRIC RING STACK

Current for the background magnet is controlled by a rate control assembly consisting of a variable speed direct current motor driving a 25-turn helipot. This permits the variation of the magnetic field from 0-30 kilogauss at rates varying from 3 gauss/second to 500 gauss/second.

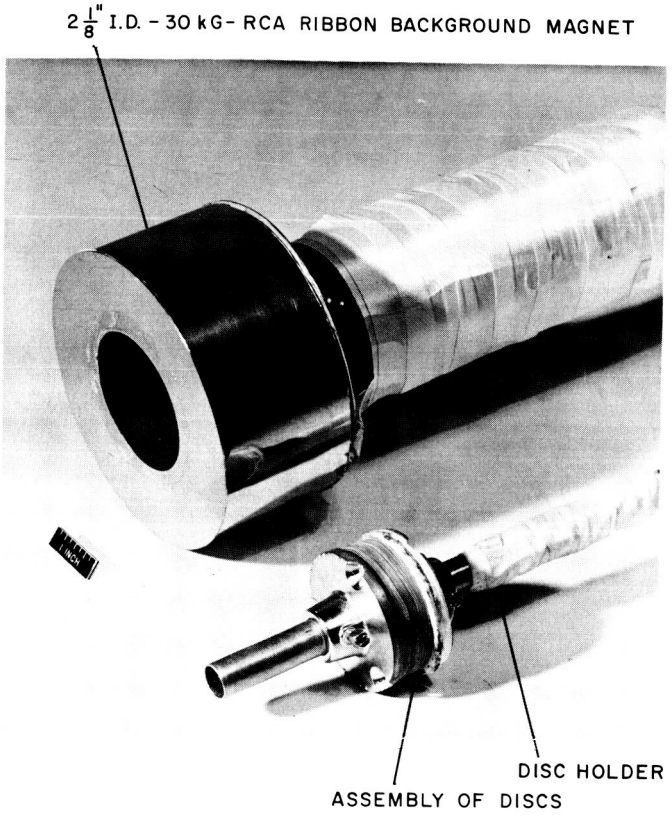

FIG. 21 A 30 kG BACKGROUND MAGNET AND CONCENTRIC RING STACK

The trapped and shielded fields obtained with various stack configurations are summarized in Table VI. A determination of and B_o was made only for the array of Test 6 and 7. In these cases B_o was minus 60 kilogauss and α was 7.8×10^9 gauss-amp./cm^2. This latter value is an average value since the stack consisted of discs processed from many different runs. The material from each run was processed somewhat differently and electromagnetic performance differed from run to run. In each of these tests it was observed that no flux jumps were present and that the trapped field in the niobium-stannide rings remained constant with no observed decay.

TABLE VI

Shielding Behavior of Stacked Discs with Concentric Nb_3Sn Rings

Test No.	Number of Discs	Length of Stack	Discs from Run Nos.	Trapped Field kG	Shielded Field kG	Rate of Field Application
1	85	0.165"	1 thru 19	7.0	5.0	70 gauss/sec.
2	177	0.321"	20-21-22	4.0	4.0	64 gauss/sec.
3	262	0.470"	1 thru 22	10.8	12.0	64 gauss/sec.
4	262 *	1.0370"	1 thru 22	8.0	9.0	60 gauss/sec.
5	160	0.264"	23	4.0	4.5	150 gauss/sec.
6	458	0.791"	1 thru 23	12.0	15.0	64 gauss/sec.
7	462 *	1.7"	1 thru 23	9.5	16.3	50 gauss/sec.

* Interleaved with mylar-copper-mylar

In tests 4 and 7, discs of sandwiched mylar (0.25 mil)-copper (0.7 mil)- mylar (0.25 mil) were alternated with the niobium-stannide discs to determine if the critical current could be enhanced. The length of the stacked array with the mylar-copper-mylar discs was doubled and the corresponding trapped field decreased from 10.8 to 8.0 and from 12 to 9.5 kilogauss respectively. No enhancement of critical current was evidenced with the mylar-copper-mylar discs indicating that the inherent maximum current capacity of the niobium-stannide had already been attained without the mylar-copper-mylar discs. In these two tests the trapped field initially decayed one and two kilogauss respectively. This decay was caused by the decay of the induced currents in the mylar-copper-mylar interleaving discs. Thereafter the trapped field remained constant.

A critical state curve of Test 7 (See Table VI) for discs is shown in Figure 21B.

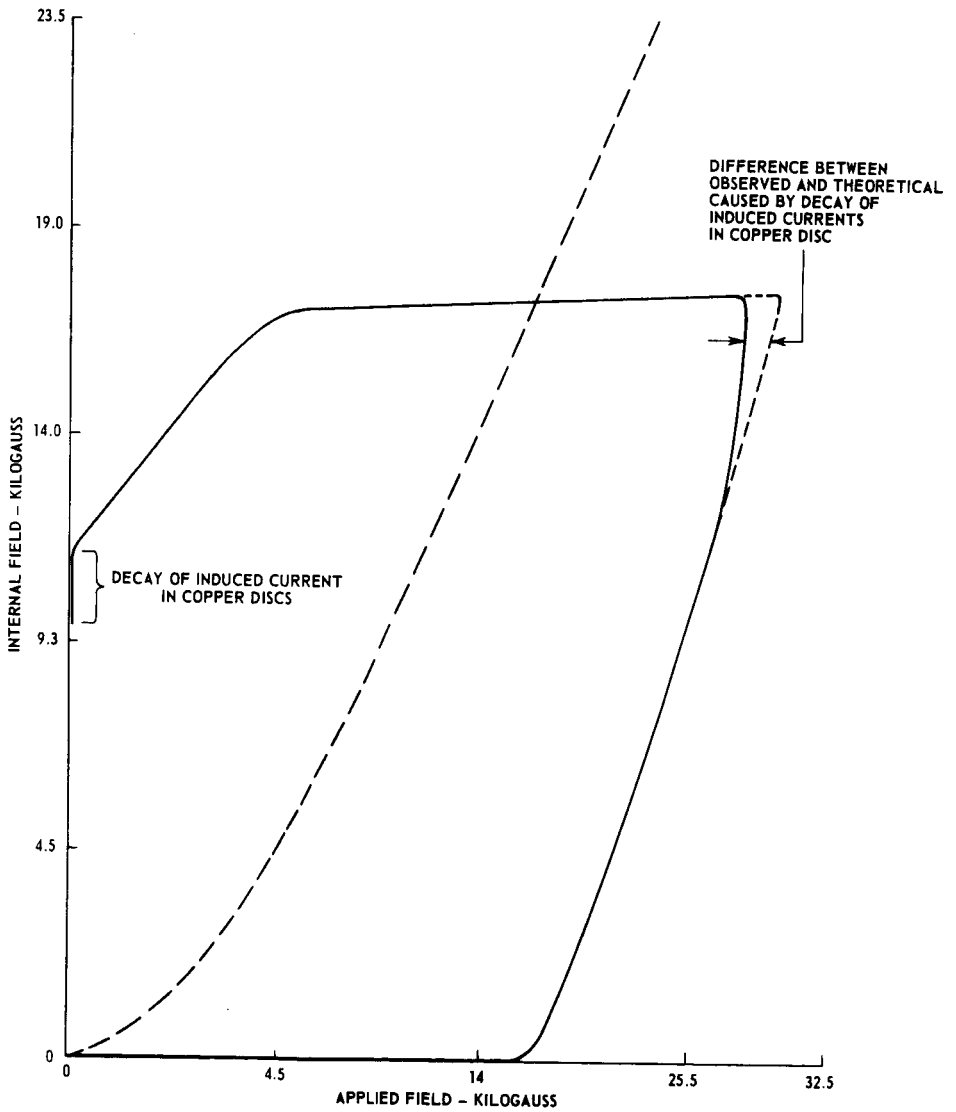

Fig.21b Critical State Curve for a Stack Concentric Rings-Test 7

Based on the observed results with these stacks, it appears that high magnetic fields in large diameter can be shielded free from flux jumps. This construction approach also presents possibilities in the construction of flux pumps, energy storage, and other superconductive devices. These will be discussed in Section VI.

V. ELECTRON IRRADIATION OF Nb_3Sn SAMPLES

A. INTRODUCTION

To determine the effects of electron irradiation on the current density of niobium-stannide, four current density specimens and one critical temperature measurement specimen were prepared. The critical current and field characteristics of each sample before electron radiation was determined. Normalcy was considered as the onset of resistance at the 10-microvolt level.

The samples were then subjected to electrons of 1 MEV energy in integrated flux densities ranging from 10^{17} to 10^{18} electrons/cm^2. By way of comparison, in the heart of the outer zone of the Van Allen Belt, 3 to 4 x 10^6, 1 MEV, electrons per cm^2 seconds equivalent to a cumulative density of only 1 x 10^{14} electrons per cm^2-year are encountered[12]. At this electron density level it would require 10,000 years to achieve the results obtained with these samples. The dimensions of the current density samples are shown in Figure 22.

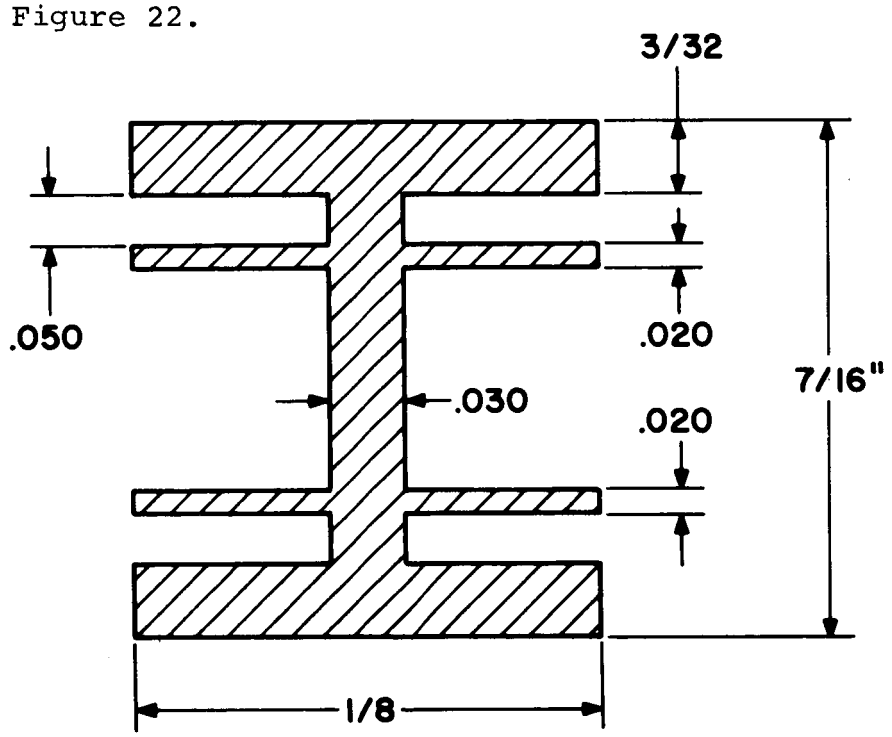

FIG. 22 ELECTRON BOMBARDMENT SPECIMEN

The niobium-stannide was deposited on a Hastelloy substrate to permit removal of heat generated by electron bombardment.

The samples were mounted on a copper block and irradiated under vacuum. A nitrogen cold finger removed from the block heat generated by the high electron current density. A thermocouple mounted on the copper block monitored sample temperature during irradiation. At no time during the irradiation was the temperature of the samples permitted to exceed 300°K.

B. EXPERIMENTAL RESULTS

Specimen 26-2A-#1 was used as a non-irradiated control and measurement of its critical current and field characteristics before and after handling did not reveal any significant difference. These results are shown in Figure 23.

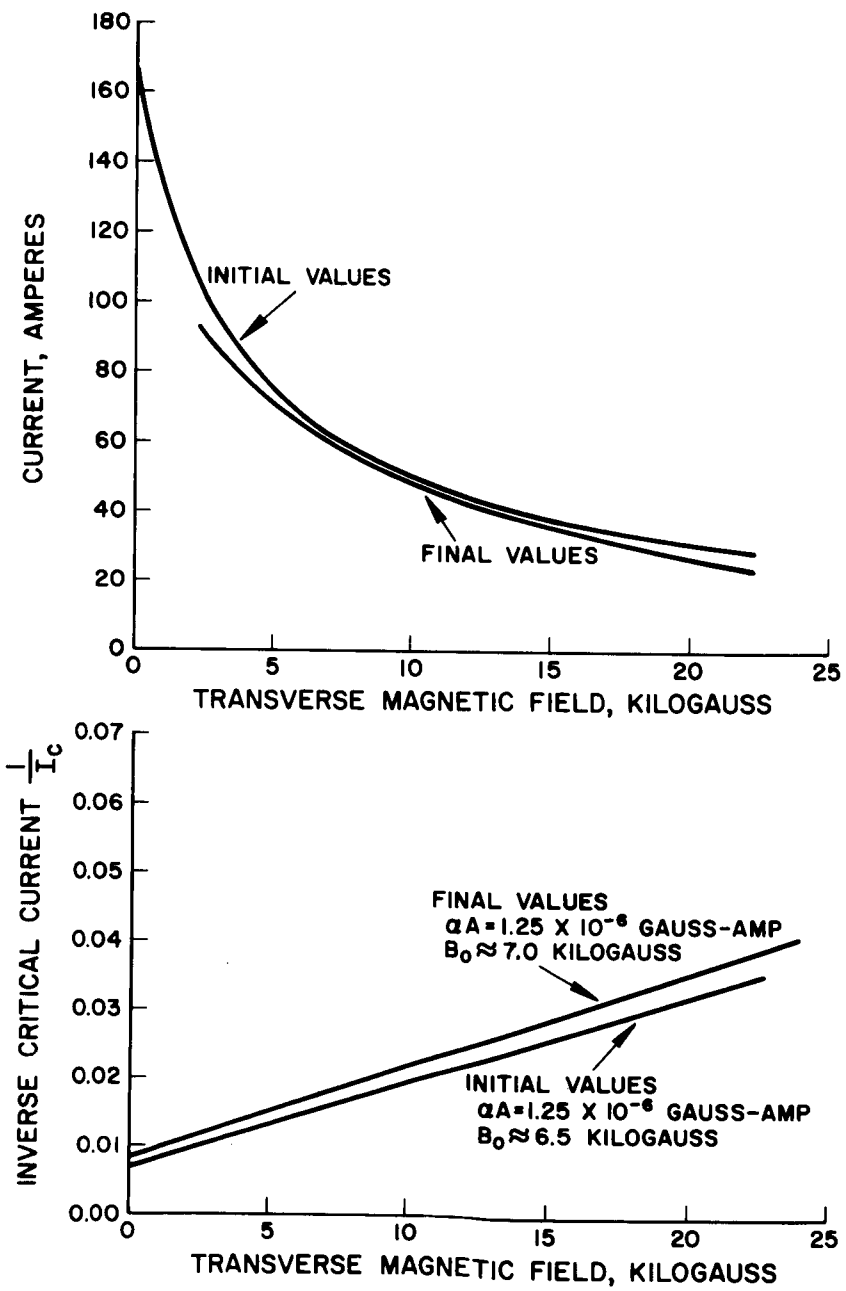

FIG. 23 EFFECT ON CURRENT DENSITY OF MOUNTING AND DISCONNECTING SAMPLE FROM IRRADIATION FIXTURE. SPECIMEN 26-2A #1

Specimen 26-2B #2 was initially irradiated to a total of 1 x 10^{17}, 1 MEV, electrons/cm^2. This irradiation level did not significantly alter the critical current performance level. Upon irradiating this same sample with an additional 10^{18} electrons/cm^2, the current level was lowered by approximately 47 percent. These results are shown in Figure 24.

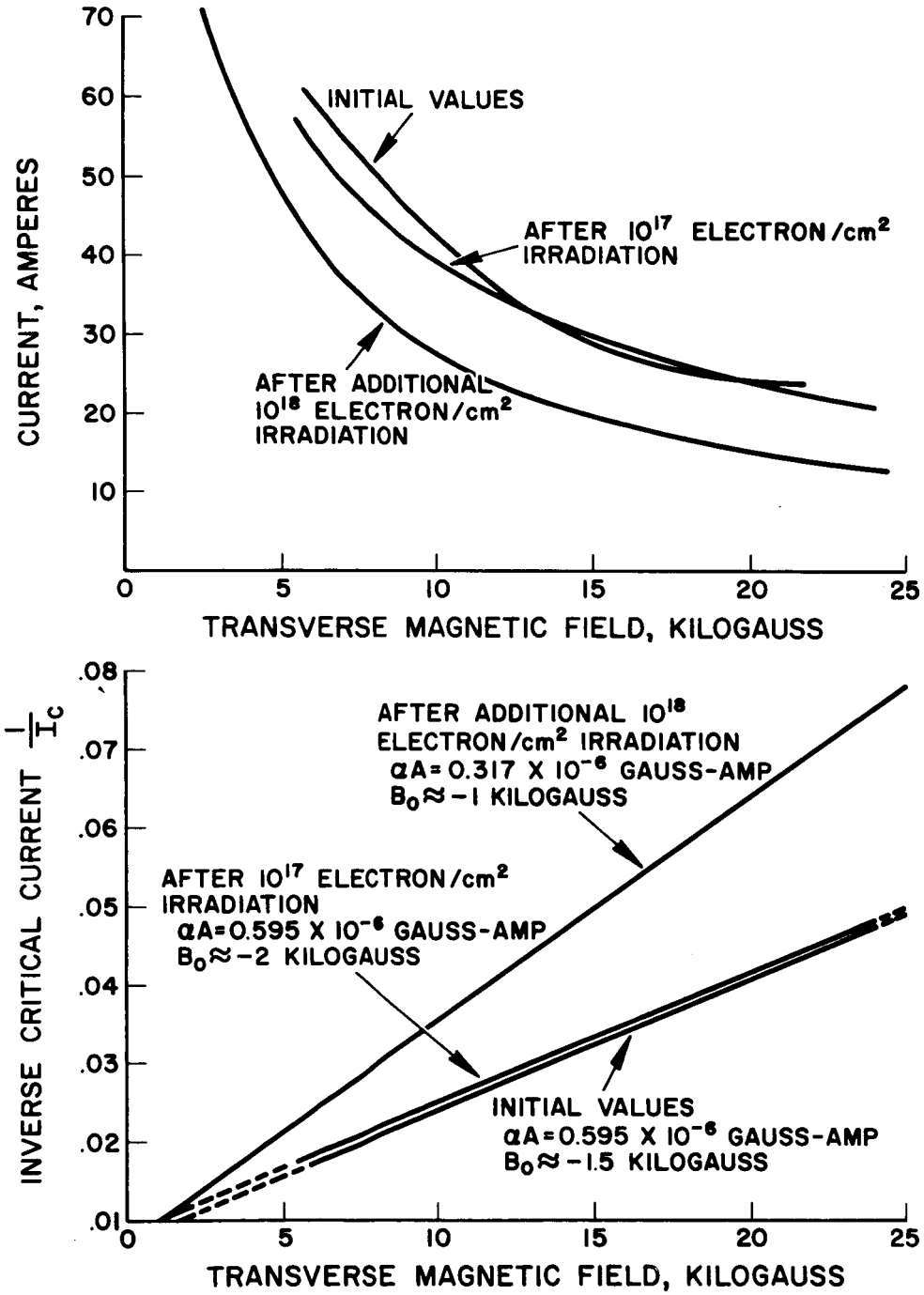

FIG. 24 EFFECT OF ELECTRON BOMBARDMENT ON CURRENT DENSITY OF Nb_3Sn. SPECIMEN 26-2B #2

Another specimen, 26-2B #1, was initially irradiated with 10^{18} MEV, electrons/cm^2 which lowered the critical current level 47 percent. Upon again irradiating this sample with an additional 10^{18}, 1 MEV, electrons/cm^2, the current level was further lowered 57 percent resulting in a total decrease in current of 73 percent from the original untreated condition. The critical current and inverse critical current as a function of transverse magnetic field are plotted in Figure 25.

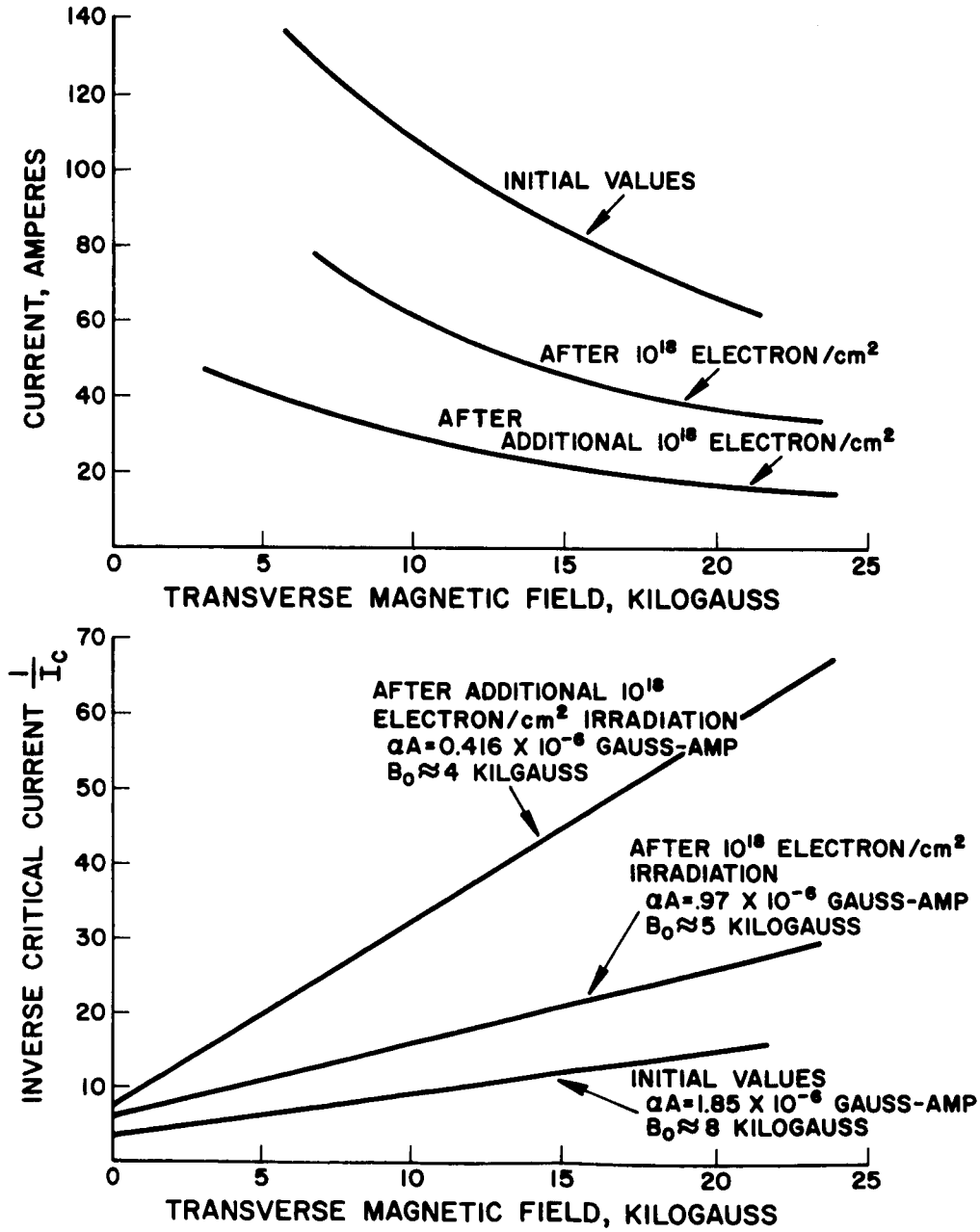

FIG. 25 EFFECT OF ELECTRON BOMBARDMENT ON CURRENT DENSITY OF Nb_3Sn. SPECIMEN 26-2B #1

Sample 26-B #3 was also irradiated with 1 x 10^{18}, 1 MEV, electron/cm^2; however, while mounting for electrical testing the sample was damaged.

The critical temperature before irradiation was 16.8° K with a 2° K transition width. After bombardment with 10^{18}, 1 MEV, electrons no difference in critical temperature was detected. These results are shown in Figure 26.

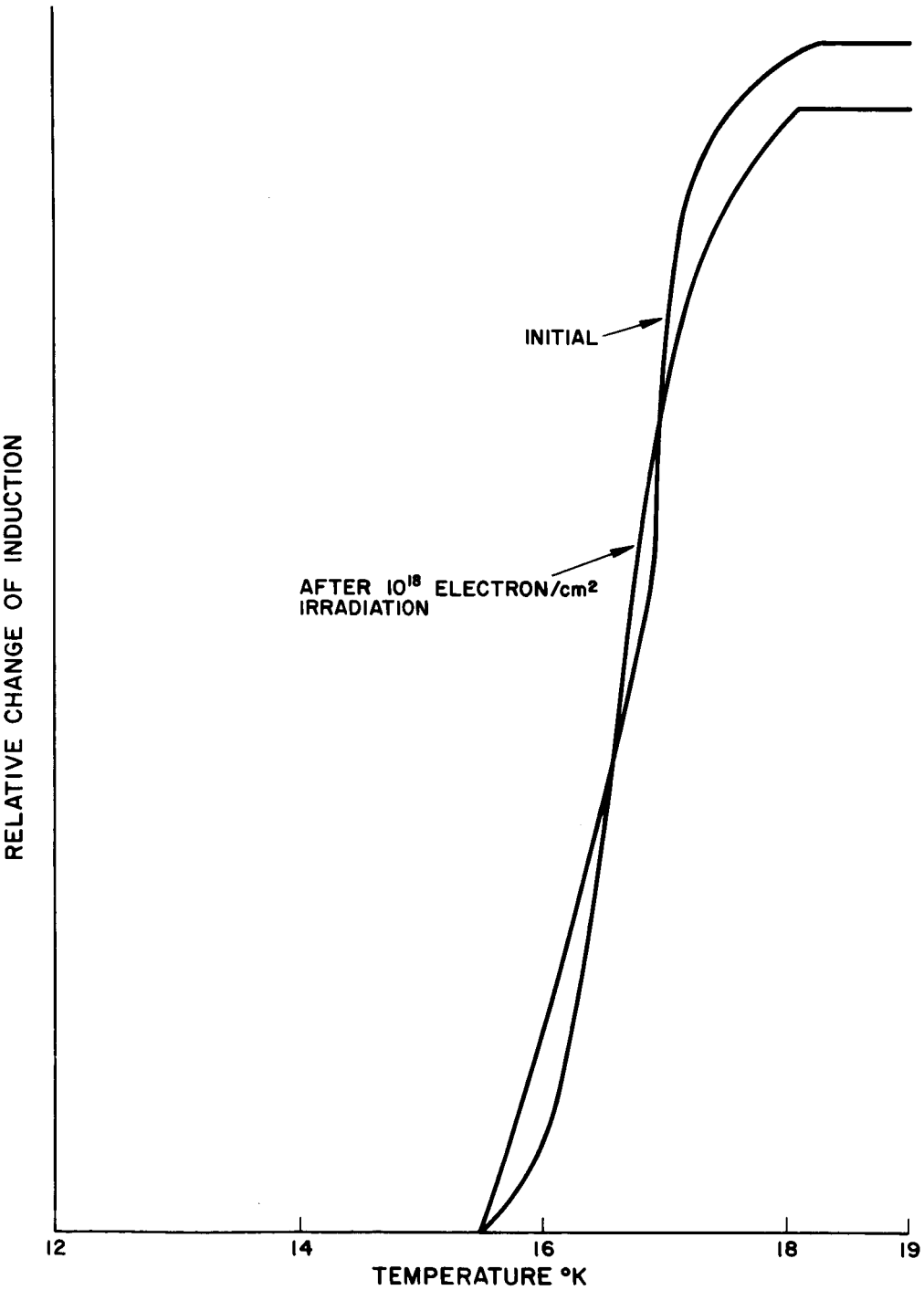

FIG. 26 EFFECT ON CRITICAL TEMPERATURE OF 10^{18} ELECTRON/cm^2 IRRADIATION

C. DISCUSSION OF RESULTS

All results described above are summarized in Table VII.

TABLE VII

Effect of Electron Irradiation on the Current Density of Nb_3Sn

Sample	Pre-Radiated A, amp-gauss	Electron Irradiation Density, Electron/cc	Cumulative Electron Density, Electron/cc	New A Amp/Gauss	Change of A	Cumulative Change from Initial A
26-2B#2	0.595×10^6	10^{17}	10^{17}	0.595×10^6	none	None
26-2B#2	0.595×10^6	10^{18}	10^{18}	0.317×10^6	47% dec.	47% dec.
26-2B#1	1.85×10^6	10^{18}	10^{18}	0.97×10^6	47% dec.	47% dec.
	0.97×10^6	10^{18}	2×10^{18}	0.42×10^6	57% dec.	73% dec.
26-2B#3	Destroyed in Testing					
26-2A#1 *	0.792×10^6	0	0	0.792×10^6	0	0

* Control Sample - mounted and handled in exactly the same manner as 26-2B#1 and 26-2B#2 except not subjected to irradiation.

The mechanism responsible for the decrease in current carrying capacity has not yet been determined. These results are quite different from the neutron irradiation results where a current increase is usually observed.[6] Crystal damage resulting from electron radiation is, however, significantly different from that of the neutron irradiation in that the former generates pinpoint defects and the latter generates line defects. In order to obtain further insight into the electron damage defects, the Lewis Research Center is performing electron micrograph cross sections of radiation samples before and after radiation to determine if structural differences can be detected. This latter work was initiated after the conclusion of this contract.

VI. APPLICATIONS

The techniques developed for depositing niobium-stannide on two-inch wide ribbon and photoengraving intricate patterns on the ribbon are equally well adaptable to a variety of devices. In addition, the flux jumping problems usually associated with these devices are minimized by maintaining thin Nb_3Sn deposits on the ribbon and separating the Nb_3Sn films by concentric insulator patterns. The following devices will be discussed in this section:

A. Magnetic field shielding
B. Magnetic field shaping
C. Permanent magnets
D. Energy storage
E. Magnetic field concentrators
F. Flux transfer pumps

A. MAGNETIC FIELD SHIELDING

Small magnetic fields (0-2 kilogauss) can readily be shielded by 0.5 to 2.0 mil thick Nb_3Sn layer. Thicker niobium-stannide deposit exhibits significant shielding instabilities. The experimental and theoretical considerations involved in this type of magnetic shielding were discussed in Section III.

In copper magnets small field fluctuations are frequently encountered resulting from magnet current fluctuations. These field fluctuations can readily be shielded by these thin Nb_3Sn coating.

To shield large magnetic fields either for space application or instruments in the vicinity of high-field magnets, the concentric Nb_3Sn ring-stacked disc approach discussed in Section IV is potentially attractive. With this type of shielding assembly, flux jumps were not encountered even at very rapid rates of field change. The concentric ring approach has been used for shielding cylindrical volumes and should be similarly suitable for shielding rectangular or other irregular volumes. With the 2-inch wide Nb_3Sn-coated ribbon, it was possible to magnetically shield rectangular areas such as 0.5 to 1.0 inch wide and any desired lengths. Larger magnetically shielded areas are believed practical but will require a somewhat wider Nb_3Sn-coated ribbon. Using the above techniques, it should be possible to shield large magnetic fields, free from flux jumps and in a variety of shapes and volumes.

B. MAGNETIC FIELD SHAPING

The Nb_3Sn superconductive rings likewise should provide a versatile manner of shaping desired magnetic fields. Stacking discs with different numbers of concentric rings will selectively shield portions of a background field. The accuracy of the shaped field can be refined to the desired degree by proper arrangement and adjustment of selected discs.

C. PERMANENT MAGNETS

Maintained at 4.2° K, the trapped magnetic field in a suitable stack of discs with concentric Nb_3Sn rings can be employed as a stable permanent magnet. Inasmuch as the concentric rings are completely superconductive with no normal contacts, magnetic field decay is not expected. Over short time periods trapped field decay in concentric Nb_3Sn ring stacks was not detected.

D. ENERGY STORAGE

The magnetic energy stored in a superconductive magnet can be used as an energy source. The time constant for the removal of this energy depends largely on the auxiliary electrical circuitry. The economics for utilizing magnetic energy depends primarily on cost, weight, and speed of energy removal. Only cost and weight factors will be discussed here. It is believed that work is being carried out elsewhere on developing techniques for practical energy removal and utilization.

In order to compare various energy storage methods, commercial nickel cadmium batteries, capacitor banks, and superconductive magnets were compared. For the batteries and capacitors standard costs [13,14,15,16,17] as available from current literature were assumed. As for the superconductive magnets Brook coils were considered (maximum inductance for given length of ribbon). For these coils, the inductance is proportional to the 1.6 power of the length of ribbon. A projected cost \$2.50 per meter of ribbon and auxiliary hardware was assumed. The over-all results are not significantly altered even if the price for the ribbon is lower by as much as 50%. The results of this cost analysis are shown in Figure 27. It is evident that superconductive magnets do not become economically advantageous in small or moderate sizes. Only very large superconductive coils, with projected costs of one million dollars, are economically favorable over batteries.

Comparison of energy storage capacity per unit weight (pound) for batteries and superconductive magnets is shown in Figure 28.

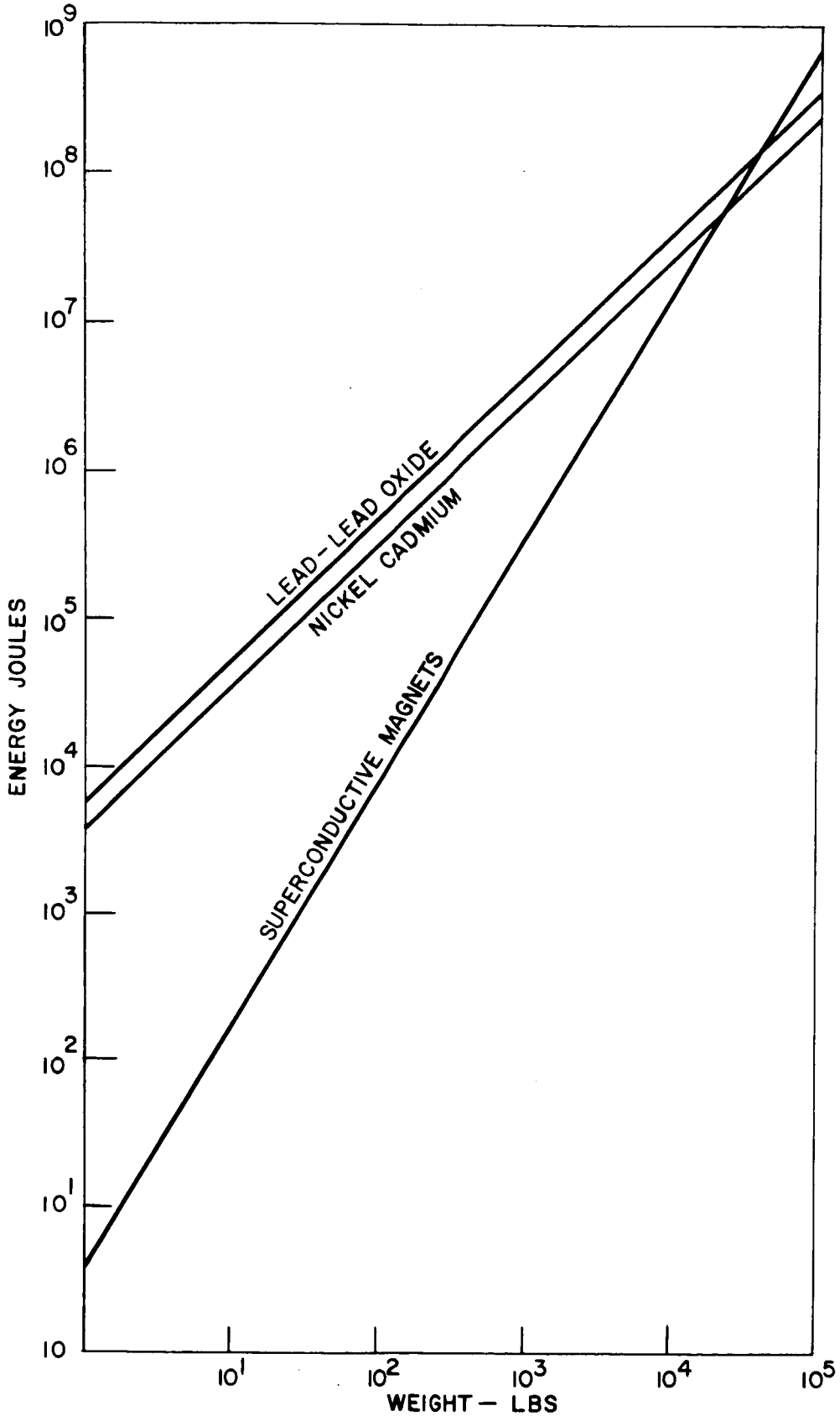

FIG.28 WEIGHT COMPARISON OF VARIOUS ENERGY STORAGE SYSTEMS

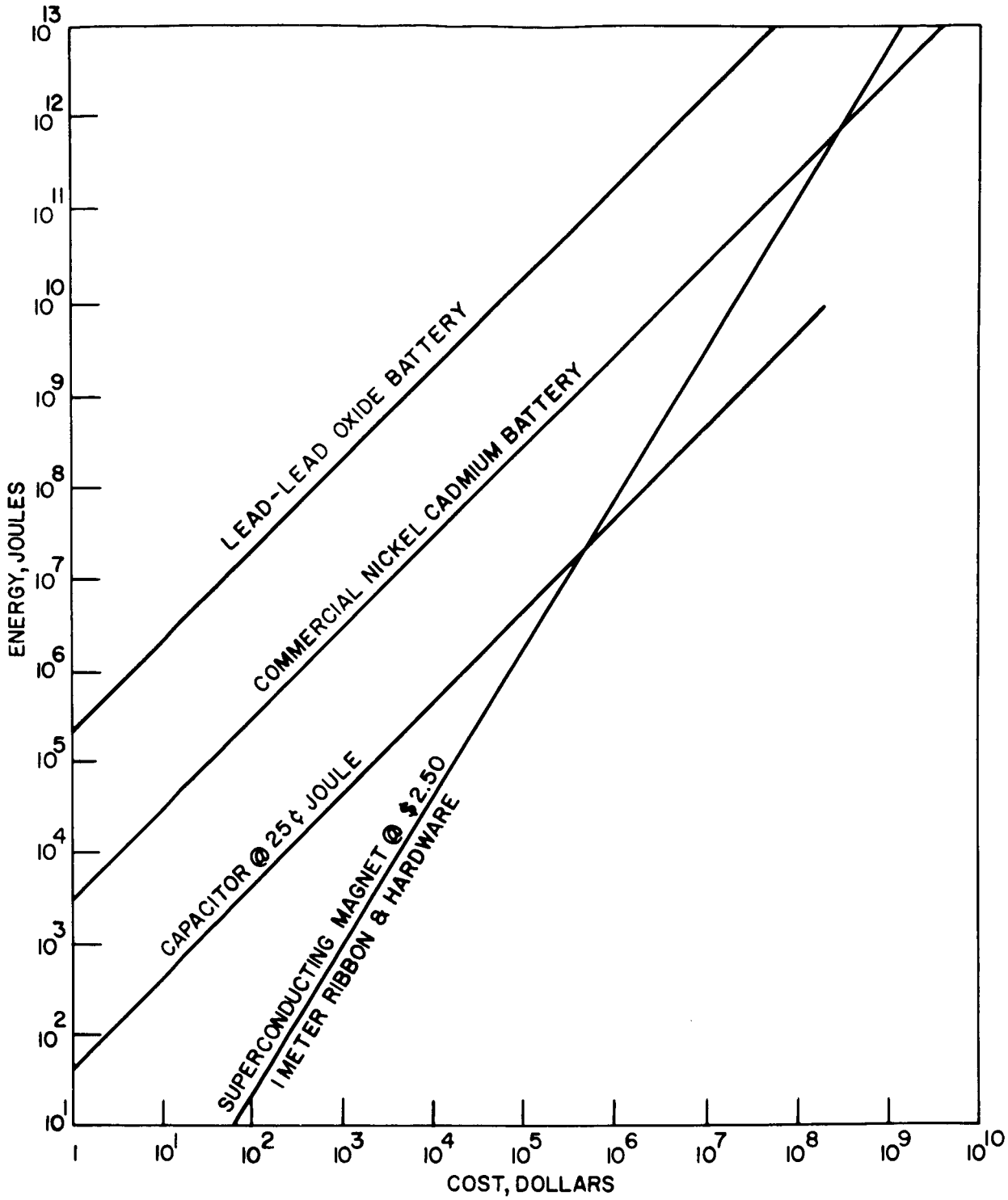

FIG.27 COST COMPARISON OF VARIOUS ENERGY STORAGE SYSTEMS

For lead acid and nickel cadmium, a capacity of 16 and 10 watt-hours per pound respectively, was assumed, and for a 1,000 meters of ribbon plus hardware a weight of six pounds was assumed. From these considerations, it appears that superconductive magnets are lighter per joule only for energy requirements exceeding 5×10^4 joules.

The above discussion was based solely on cost and weight considerations. However, other considerations such as speed of energy release (time constant), efficiency of energy release, and volume of the entire system should also be carefully considered.

E. MAGNETIC FIELD CONCENTRATORS[18]

The techniques developed for depositing Nb_3Sn on 2-inch wide ribbon and chemically etching should be applicable for field concentrating devices. Such a device consists of a stack of solenoidial discs. One of these discs is shown in Figure 29.

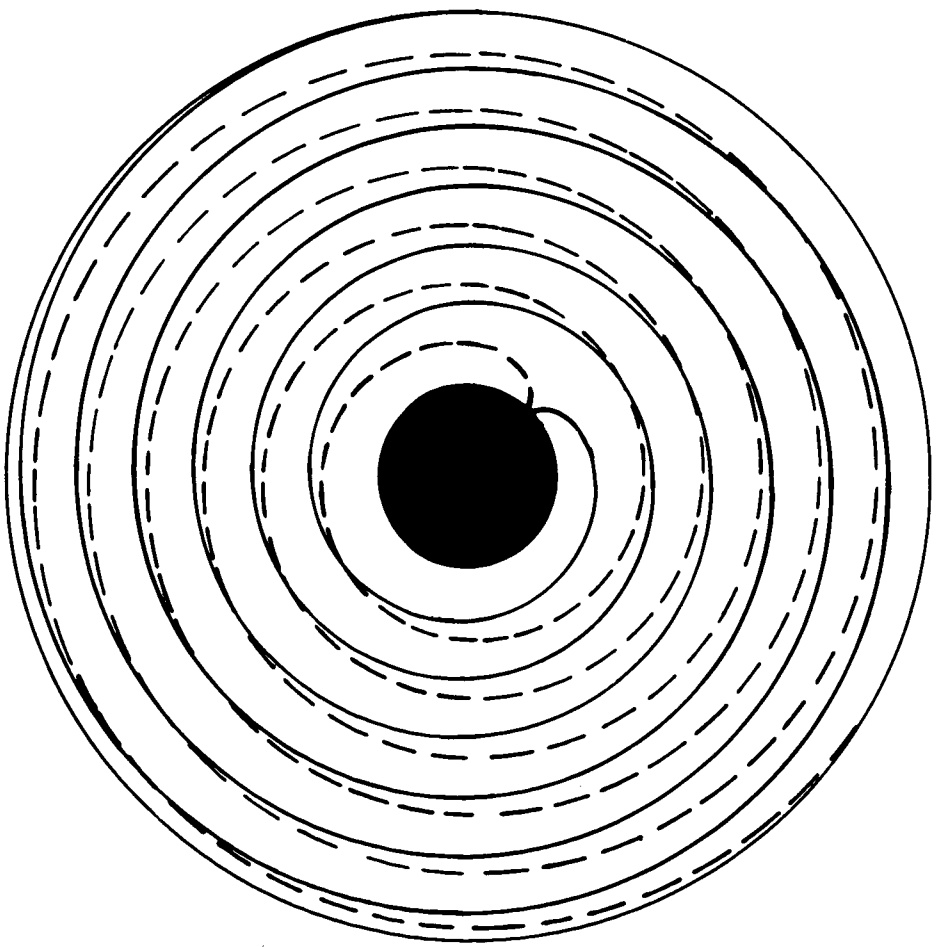

FIG. 29 SOLENOID DISC

The solenoidial ring is continuous from side to side with no normal contacts. When placed in a background field, persistent currents are induced in the outer ring. Since these rings are continuous, this current flows from the outside to the inner portion of the disc. Due to the geometrical configuration of the solenoid, the current in the center contributes more to the field than the current on the outside. Consequently, as the background field is initially increased, the induced current will generate a total field in the center opposite to the applied field as shown in Figure 30 from 0 to 1.

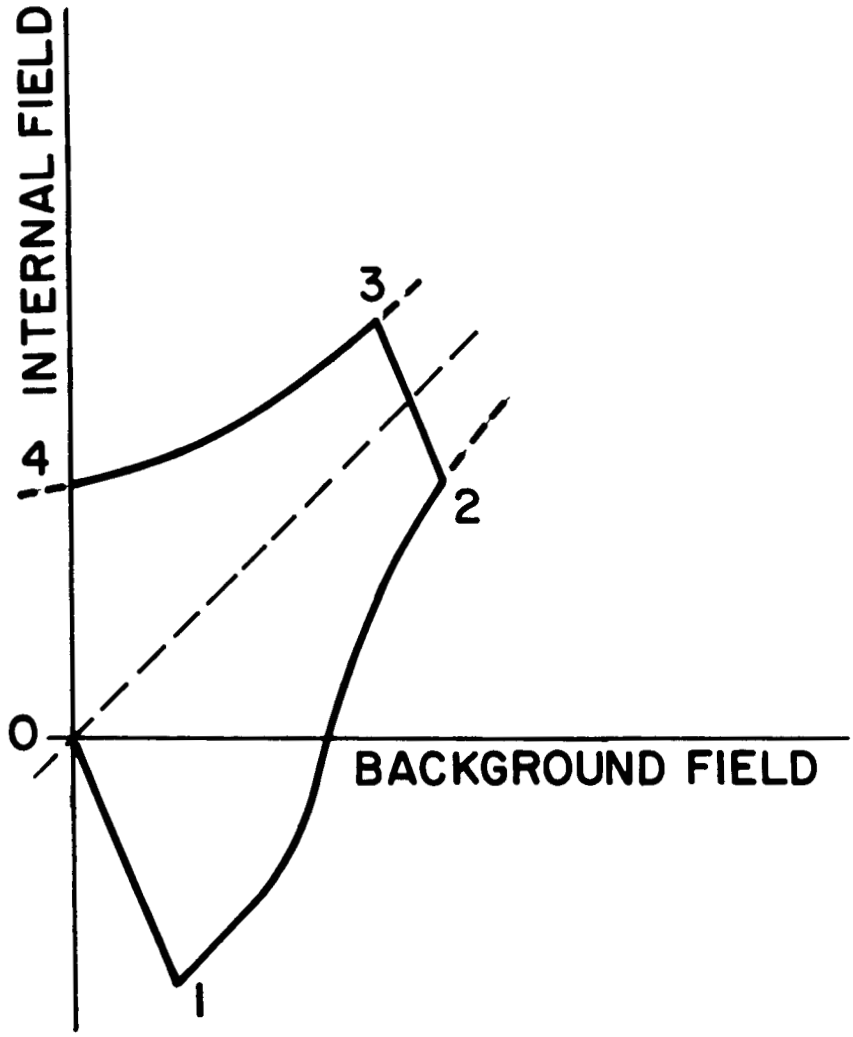

FIG. 30 CRITICAL STATE CURVE OF STACK OF SOLENOID DISCS

After the critical state curve is reached, the shielded field will decrease at higher fields as shown from 1 to 2. Upon decreasing the background field, the magnitude of the induced current is initially decreased, then reversed as shown from 2 to 3. At point "3", the field at the center is higher than the maximum background magnetic field. The degree to which the field can be concentrated is dependent upon the stack configuration. As the field if further decreased, the trapped field decreases from point "3" to "4".

F. FLUX TRANSFER AND PUMPING

The Nb_3Sn deposition and photoetching is considered applicable also for flux transfer from a small volume to a larger volume, and pumping a low intensity magnetic field to obtain a higher magnetic field. By using the individual ring structure, the flux jumping problem can either be minimized or even completely alleviated. Consider the individual sheet as shown in Figure 31 and assembled as shown in Figure 32. "S1" and "S2" are switches assembled such that a heater wire loops each sheet as indicated.

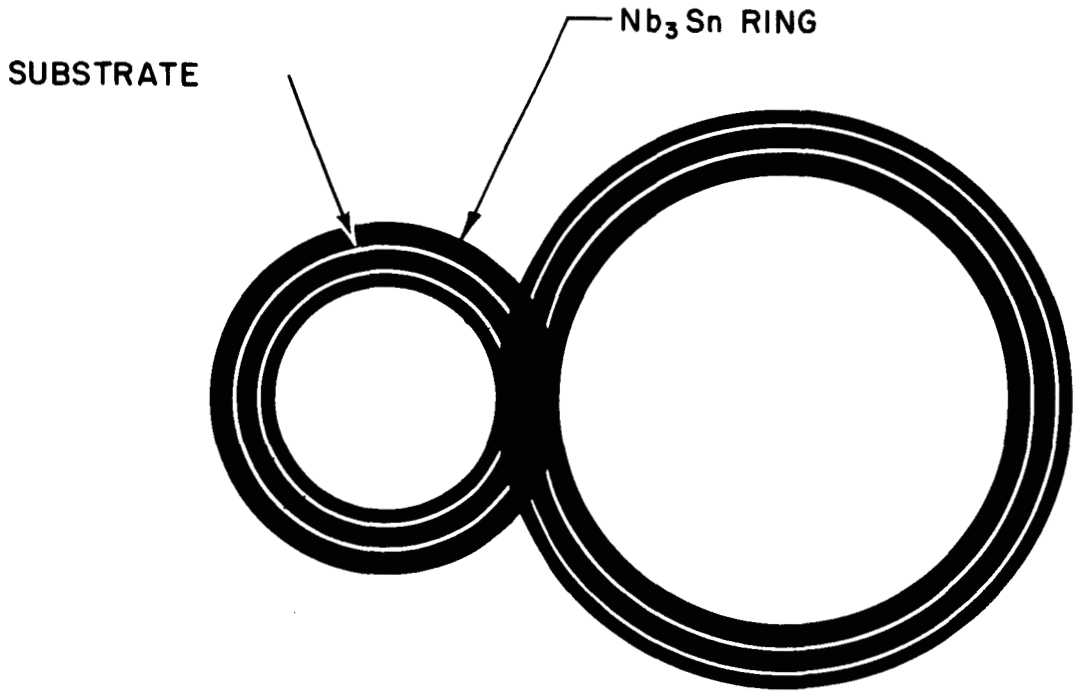

FIG. 31 FLUX TRANSFER MECHANISM

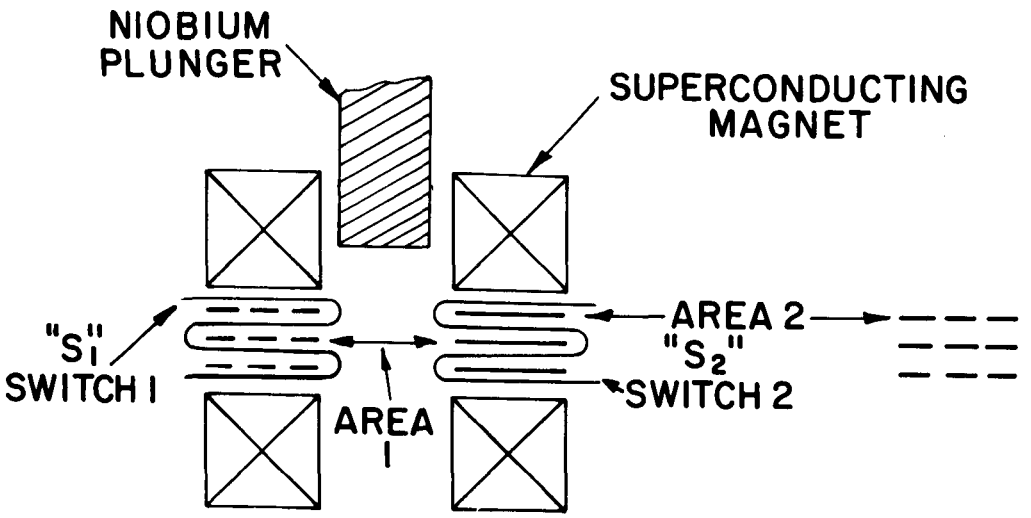

FIG. 32 STACK OF FLUX TRANSFER SHEETS

The flux transferring operating is as follows:

1. Initially "S1" is on and the superconductor is normal. "S2" is off and the Nb_3Sn is superconductive.

2. The maximum magnetic field (H_m) produced by the background magnet is applied.

3. "S1" is now turned off and the Nb_3Sn is made superconductive. The applied field is decreased inducing current in the small loops.

4. "S2" is then turned on and the Nb_3Sn bounded by "S2" is normal. This result in the sharing of the magnetic field between area 1 and area 2. The field in area 2 is then given by:

$$H_2 = \frac{A_1 H_m}{A_1 + A_2}$$

5. "S2" is now turned off and the Nb_3Sn bounded by "S2" becomes superconductive. "S1" is turned on switching the Nb_3Sn bounded by "S1" into the normal state.

6. The background field is then again increased and steps 1 to 5 repeated. The new field H_2' in A_2 is now given by:

$$H_2' = \frac{A_1 H_m + A_2 H_2}{A_1 + A_2}$$

7. Again repeating steps 1 to 5 gives a field of

$$H_2'' = \frac{A_1 H_m + A_2 H_2'}{A_1 + A_2}$$

It is readily seen that $H_2'' > H_2' > H_2$ consequently, the magnetic field in area 2 is gradually pumped to that of area 1. By inserting a superconductor plunger such as niobium shown in Figure 32 provided the critical field of niobium is not exceeded, the magnetic field is squeezed and a new maximum magnetic field is developed which is given by:

$$H_m' = \frac{A_1 H_m}{A_1 - A_{plumger}}$$

with this new H_m', the flux transferring action indicated by steps 1 to 5 can again be repeated, and a field approaching H_m' will eventually be transferred to A_2.

VII. ACKNOWLEDGEMENT

The authors acknowledge the assistance of Dr. R. L. Novak in electron irradiating the Nb_3Sn samples. They also wish to note the assistance of Mr. S. Husni in the plating of the cylinder and ribbon, and the etching of the concentric rings. In addition, the authors are grateful for the continuous assistance of Mr. R. Berger in the preparation of niobium stannide layers on cylinders and in the deposition of Nb_3Sn on the 2-inch wide ribbon, and Mr. G. Storch for assistance in the electro-magnetic evaluation of niobium stannide layer and ribbon.

VI. REFERENCES

1. Contract No. AF 33(616-6405) Physics Lab. A.S.D. Wright-Patterson Air Force Base

2. J. J. Hanak, Vapor Deposition of Nb_3Sn, Metallurgical Society Conference 19, 161 (1962)

3. G. W. Cullen, Private Communication

4. J. J. Hanak, J. Metals 16, 97 (1964)

5. J. P. McEnvoy, Jr. and R. F. Decel, Applied Physics Letters, 4, 43, 1964

6. G. W. Cullen, R. L. Novak, J. P. McEnvoy, RCA Review, Vol. XXV, 479 (September, 1964)

7. B. D. Cullidy, Elements of X-ray Diffraction, Pages 324-344, Addison-Wesley, 1956

8. Y. P. Kim, C. F. Hempstead and A. R. Strnad, Physics Review 129, 528 (1963)

9. C. R. Wischmeyer, Y. P. Kim, Bulletin A.P.S., 1964 Spring Meeting EF 10, 439

10. J. J. Hanak, RCA Review, Vol. XXV, 551 (September, 1964)

11. R. W. Boom, R. S. Livingston, Superconducting Solenoids, Proceedings of the IRE, March, 1962

12. Frank L. Bouquet, Jr., Space Aeronautics, May, 1963

13. Sears-Roebuck Catalogue

14. Yardney Electric Corporation Price Catalogue

15. Gould National Batteries, Inc. Price Catalogue

16. Commercial Available Pulsing Equipment

17. C. K. Morehouse, R. Glicksman, and G. S. Lozier, "Batteries", Proceedings IRE, Vol. 46, Pages 1462-1483; August, 1958

18. J. J. Hanak, Private Communication

FINAL DISTRIBUTION LIST
Contract NAS 3-4113

NASA-Lewis Research Center
21000 Brookpark Road
Cleveland, Ohio 44135
Attn: Spacecraft Technology Division
Albert E. Anglin (8)
James C. Laurence (2)
J. Howard Childs (1)
D. Lockwood (1)

NASA-Lewis Research Center
21000 Brookpark Road
Cleveland, Ohio 44135
Attn: Electric Propulsion Laboratory
W. E. Moeckel (1)
E. E. Callaghan (1)

NASA-Lewis Research Center
21000 Brookpark Road
Cleveland, Ohio 44135
Attn: Spacecraft Technology Procurement Section (1)

NASA-Lewis Research Center
21000 Brookpark Road
Cleveland, Ohio 44135
Attn: Technology Utilization Office (1)

NASA-Lewis Research Center
21000 Brookpark Road
Cleveland, Ohio 44135
Attn: Library (2)

NASA Headquarters
FOB-10B
600 Independence Avenue, N.E.
Washington, D.C.
Attn: RNT/J. Lazar (2)

Aeronautical Systems Division
Wright-Patterson AFB, Ohio
Attn: ASRTCE/Harold K. Trinkle (1)

Aeronautical Systems Division
Wright-Patterson AFB, Ohio
Attn: AFAPL(APIE-2)/Charles Oberley (1)

Aeronautical Systems Division
Directorate of Materials and Processes
Wright-Patterson AFB, Ohio (1)

NASA-Langley Research Center
Langley Station
Hampton, Virginia
Attn: Library (1)

National Magnet Laboratory
M.I.T.
Cambridge, Massachusetts 02139
Attn: Mr. D. Bruce Montgomery (1)

Metallurgy Department
M.I.T.
Cambridge, Massachusetts 02139
Attn: Prof. John Wulff (1)

Oak Ridge National Laboratory
Oak Ridge, Tennessee
Attn: Mr. W. F. Gauster (1)

National Bureau of Standards
Washington, D.C. 20013
Attn: Dr. Richard Kipshot (1)

National Research Corporation
70 Memorial Drive
Cambridge, Massachusetts 02142
Attn: Technical Information Center (1)

Materials Research Corporation
Orangeburg, New York 10962
Attn: Mr. Vernon E. Adler (1)

Westinghouse Astronuclear Labs.
Electric Propulsion Laboratory
Pittsburgh, Pennsylvania 15234
Attn: Mr. H. W. Szymanowski (1)

Space Technology Laboratories
8433 Fallbrook
Canoga Park, California
Attention: Library (1)

Jet Propulsion Laboratory
4800 Oak Grove Drive
Pasadena, California 91102
Attn: Mr. John Paulson (1)

Aerospace Corporation
P.O. Box 95085
Los Angeles, California 90045
Attn: Library Technical Documents Group (1)

General Electric Company
Advanced Technology Laboratories
1 River Road
Schenectady, N. Y. 12305
Attn: Mr. R. W. Hardt (1)

Linde Company
Div. of Union Carbide Corp.
270 Park Avenue
New York, N. Y. 10017
Attn: Mr. N. B. Broune (1)

NASA-Marshall Space Flight Center
Huntsville, Alabama 35812
Attn: Mr. Eugene W. Urban (1)

Westinghouse Electric Corporation
55 Public Square
Cleveland, Ohio 44113
Attn: Mr. Steve A. Cifani (1)

AVCO-Everett Research Laboratory
2385 Revere Beach Parkway
Everett 49, Massachusetts
Attn: Dr. Z. J. J. Stekly (1)

Atomic International Division
North American Aviation
P.O. Box 309
Canoga Park, California
Attn: Dr. R. Boom (1)

Westinghouse Electric Corporation
Research and Development Center
Pittsburgh, Pennsylvania 15235
Attn: Dr. S. Autler (1)

U. S. Atomic Energy Commission
Washington, D. C. 20545
Attn: Mr. William C. Gough (1)

NASA-Scientific & Technical Information Facility
Box 5700
Bethesda 14, Maryland
Attn: NASA Representative RQT-2448 (6)

AFWL
Kirtland Air Force Base, New Mexico
Attn: Capt. C. F. Ellis/WLPC (1)

NASA-Lewis Research Center
21000 Brookpark Road
Clevelandl Ohio 44135
Attn: Reports Control Office (1)